ELSEVIER

Journal of Molecular Structure (Theochem) 573 (2001) 91–128

THEO CHEM

www.elsevier.com/locate/theochem

Research activities of the theoretical chemistry group at the University of Tokyo

Haruyuki Nakano, Takahito Nakajima, Takao Tsuneda, Kimihiko Hirao*

Department of Applied Chemistry, Graduate School of Engineering, The University of Tokyo, Tokyo 113-8656, Japan

Received 22 February 2001; revised 18 April 2001; accepted 23 April 2001

Abstract

One of the authors (Kimihiko Hirao) was invited to the University of Tokyo in 1993 as the first professor of theoretical chemistry. Since then, our quantum chemistry research group has grown larger and larger and has now become one of the centers of theoretical chemistry in Japan. We are aiming at developing accurate molecular theory on systems containing hundreds of atoms. We continue our research in the following three directions: (i) development of new ab initio theory, particularly multireference-based perturbation theory; (ii) development of molecular theory including relativistic effects; and (iii) development of exchange and correlation functionals in density functional theory. We have enjoyed good progress in each of the above areas. We are very excited about our discoveries of new theory and new algorithms and we would like to share this enthusiasm with readers. The present review is a summary of our research activities achieved in the last 5 years.

Keywords: Multireference based perturbation theory; Density functional theory; Relativistic theory; MRMP; MC-QDPT; RESC; Higher order Douglas–Kroll approximation; OP correlation functional; Parameter-free exchange functional

1. Multireference perturbation theory

One of the most important advances in the last decades in electronic structure theory is the development of the multireference technique, i.e. the multiconfiguration self-consistent field (MCSCF) method, and configuration interaction (CI), coupled cluster (CC), and perturbation methods based on the MCSCF functions. These methods now play a central role in the study of electronic structure of molecules and chemical reaction mechanisms, especially in those concerned with electronic excited states.

Among the several types of MCSCF methods, CASSCF is commonly used at present. In fact, it has many attractive features: (1) applicable to excited states as well as the ground state in a single framework; (2) size-consistent; and (3) well-defined on the whole potential energy surface if an appropriate active space is selected. However, CASSCF takes into account only non-dynamic electron correlation and not dynamic correlation. The accuracy in energies such as the excitation energy and dissociation energy does not reach chemical accuracy, that is, within several kcal/mol. A method is necessary that takes into account both the non-dynamic and dynamic correlations for a quantitative description.

Our MRMP (multireference Møller–Plesset) perturbation method [1–4] and MC-QDPT (quasi-degenerate perturbation theory with multiconfiguration self-consistent field reference functions)

* Corresponding author. Tel.: +81-3-5841-7223; fax: +81-3-5841-7241.

E-mail address: hirao@qcl.t.u-tokyo.ac.jp (K. Hirao).

0166-1280/01/$ - see front matter
PII: S0166-1280(01)00546-2

[5,6]are perturbation methods of such a type. In these methods, the CASSCF wavefunctions are first determined, and the perturbation calculation is done with those wavefunctions used as reference (zeroth-order wavefunctions) based on Rayleigh–Schrödinger perturbation theory (PT) in MRMP and van Vleck PT in MC-QDPT. These PTs have many attractive features:

1. generally applicable to a wide class of problems and a wide variety of molecules in a single framework;
2. almost size-consistent;
3. applicable to excited states and open-shells as well as the ground state;
4. stable on the whole potential surface if the reference CASSCF function is appropriately chosen;
5. accurate enough to provide chemical accuracy. Although MRMP and MC-QDPT at the lowest non-trivial order (the second order) does not yield a very close total energy to the exact one, they are well balanced. Relative energies such as dissociation energies, excitation energies, and activation energy are quite good.
6. Much more efficient and handy than MRCI and MRCC methods. The energy is computed as a sum of the product of molecular integrals and coupling constants between the target state and CSF divided by the energy difference. The resource required does not depend strongly on the size of the active space and basis set. This presents a significant contrast to the case of MRCI and MRCC.

In this section, we show the formalism of multireference perturbation theory and some applications to potential energy surfaces and electronic excited spectra.

1.1. The MRMP method—Multireference Møller–Plesset perturbation method [1–4]

Our basic problem is to find approximations to some low-lying solutions of the exact Schrödinger equation:

$$H\Psi = E\Psi. \tag{1}$$

H is the Hamiltonian and it is decomposed into two parts, a zeroth-order Hamiltonian H_0 and a perturbation V:

$$H = H_0 + V. \tag{2}$$

We assume that a complete set of orthonormal eigenfunctions $\{\Psi_i^{(0)}\}$ and their corresponding eigenvalues are available:

$$H_0\Psi_i^{(0)} = E_i^{(0)}\Psi_i^{(0)}. \tag{3}$$

Then the state wavefunction Ψ_I is expanded in terms of basis functions $\Psi_k^{(0)}$ as:

$$\Psi_I = \sum_k C_{Ik}\Psi_k^{(0)}. \tag{4}$$

Some of the basis functions define an active space P, and the remaining part of Hilbert space is called the orthogonal space $Q = 1 - P$. The active space is spanned by the basis functions that have a filled core and the remaining active electrons are distributed over a set of active orbitals. The orthogonal complete space incorporates all other possible basis functions that are characterized by having at least one vacancy in a core orbital. The state wavefunction in an active space is written as:

$$\Psi_I^{(0)} = \sum_k C_k\Phi_k, \tag{5}$$

where the sum runs over active space basis functions $\{\Phi_i\}$ and C_k are the coefficients of only the active space basis functions. It is convenient to use intermediate normalization, that is:

$$\langle\Psi_I^{(0)}|\Psi_I^{(0)}\rangle = \langle\Psi_I^{(0)}|\Psi_I\rangle = 1. \tag{6}$$

We also assume that $\Psi_I^{(0)}$ is diagonal in P space:

$$\langle\Psi_I^{(0)}|H|\Psi_J^{(0)}\rangle = \delta_{IJ}(E_I^{(0)} + E_I^{(1)}), \tag{7}$$

with:

$$E_I^{(0)} = \langle\Psi_I^{(0)}|H_0|\Psi_I^{(0)}\rangle, \tag{8}$$

$$E_I^{(1)} = \langle\Psi_I^{(0)}|V|\Psi_I^{(0)}\rangle. \tag{9}$$

The state-specific Rayleigh–Schrödinger perturbation theory based on the unperturbed eigenvalue equation:

$$H_0\Psi_I^{(0)} = E_I^{(0)}\Psi_I^{(0)} \tag{10}$$

leads to the first $E_I^{(k)}$ as:

$$E_I^{(2)} = \langle\Psi_I^{(0)}|VRV|\Psi_I^{(0)}\rangle, \tag{11}$$

$$E_I^{(3)} = \langle \Psi_I^{(0)} | VR(V - E_I^{(1)})RV | \Psi_I^{(0)} \rangle, \tag{12}$$

$$\begin{aligned} E_I^{(4)} = {} & \langle \Psi_I^{(0)} | VR(V - E_I^{(1)})R(V - E_I^{(1)})RV | \Psi_I^{(0)} \rangle \\ & - E_I^{(2)} [\langle \Psi_I^{(0)} | VR^2 V | \Psi_I^{(0)} \rangle \\ & + \langle \Psi_I^{(0)} | VRH_0 SH_0 RV | \Psi_I^{(0)} \rangle], \end{aligned} \tag{13}$$

etc.

The R and S are the resolvent operators:

$$R = Q/(E_I^{(0)} - H_0), \tag{14}$$

$$S = P'/(E_I^{(0)} - H_0), \tag{15}$$

where $P' = P - |\Psi_I^{(0)}\rangle\langle\Psi_I^{(0)}|$.

The $E_I^{(0)}$ is given in terms of orbital energies as:

$$E_I^{(0)} = \sum_k D_{kk} \epsilon_k, \tag{16}$$

and the orbital energies are defined as:

$$\epsilon_i = \langle \varphi_i | F | \varphi_i \rangle \tag{17}$$

with:

$$F_{ij} = h_{ij} + \sum_{kl} D_{kl} \left[(ij|kl) - \frac{1}{2}(ik|lj) \right], \tag{18}$$

where D_{ij} is the one-electron density matrix. The MCSCF orbitals are resolved to make the F_{ij} matrix as diagonal as possible. This zeroth-order Hamiltonian is closely analogous to the closed-shell Fock operator. The definition of an active space, the choices of active orbitals, and the specification of the zeroth-order Hamiltonian completely determine the perturbation approximation.

When a CASSCF wavefunction is used as the reference, the zeroth plus first-order energy $E_I^{(0)} + E_I^{(1)}$ is equal to the CASSCF energy. The lowest non-trivial order is, therefore, the second order. Let the reference function $|\Psi_\alpha^{(0)}\rangle$ be a CASSCF wavefunction:

$$|\alpha\rangle = \sum_A C_A |A\rangle. \tag{19}$$

The energy up to the second order in MRMP is given by:

$$E_\alpha^{(0-2)} = E_\alpha^{\mathrm{CAS}} + \sum_I \frac{\langle \alpha|V|I\rangle\langle\alpha|V|I\rangle}{E_\alpha^{(0)} - E_I^{(0)}}, \tag{20}$$

where $\{|I\rangle\}$ is the set of all singly and doubly excited configurations from the reference configurations in CAS. The first term on the RHS is the CAS-CI energy.

1.2. MC-QDPT—Multistate multireference perturbation method [5,6]

We have also proposed a multistate multireference perturbation theory, the quasi-degenerate perturbation theory with MCSCF reference functions (MC-QDPT). In this PT, state-averaged CASSCF is first performed on a set of reference functions, and then an effective Hamiltonian is constructed, which is finally diagonalized to obtain the energies of interest. This theory includes MRMP PT (the case that the set of reference functions reduces to a single function).

The effective Hamiltonian to second order is given by:

$$\begin{aligned} (K_{\mathrm{eff}}^{(0-2)})_{\alpha\beta} = {} & \langle \alpha|H|\beta\rangle \\ & + \frac{1}{2} \sum_I \left\{ \frac{\langle \alpha|V|I\rangle\langle\alpha|V|\beta\rangle}{E_\beta^{(0)} - E_I^{(0)}} + \frac{\langle \beta|V|I\rangle\langle I|V|\alpha\rangle}{E_\alpha^{(0)} - E_I^{(0)}} \right\}. \end{aligned} \tag{21}$$

Substituting the second-quantized operator into V, we obtain an explicit formula using molecular integrals and orbital energies instead of matrix elements:

$$\begin{aligned} (K_{\mathrm{eff}}^{(0-2)})_{\alpha\beta} = {} & E_\alpha^{\mathrm{CAS}} \delta_{\alpha\beta} \\ & - \sum_{pq,B} \langle \alpha|E_{pq}|B\rangle C_B(\beta) \sum_e \frac{u_{pe}u_{eq}}{\epsilon_e - \epsilon_q + \Delta E_{B\alpha}} \\ & - \sum_{pqrs,B} \langle \alpha|E_{pq,rs}|B\rangle C_B(\beta) \\ & \times \left[\sum_e \frac{u_{pe} g_{eqrs}}{\epsilon_e - \epsilon_q + \epsilon_r - \epsilon_s + \Delta E_{B\alpha}} \right. \\ & + \sum_e \frac{g_{pers} u_{eq}}{\epsilon_e - \epsilon_q + \Delta E_{B\alpha}} \\ & \left. + \frac{1}{2} \sum_{(a,b)} \frac{g_{parb} g_{aqbs}}{\epsilon_a - \epsilon_q + \epsilon_b - \epsilon_s + \Delta E_{B\alpha}} \right] \\ & - \sum_{pqrstu,B} \langle \alpha|E_{pq,rs,tu}|B\rangle C_B(\beta) \\ & \times \sum_e \frac{g_{pers} g_{eqtu}}{\epsilon_e - \epsilon_q + \epsilon_t - \epsilon_u + \Delta E_{B\alpha}} + (\alpha \leftrightarrow \beta) \end{aligned} \tag{22}$$

with:

$$g_{pqrs} = (pq|rs) \tag{23}$$

Table 1
CASSCF and MRMP classical barrier height (kcal/mol) for the reaction $H_2CO \rightarrow H_2 + CO$. Values in parentheses include the zero point energy correction

Method Basis set/Active space	Barrier height CASSCF	 MRMP
cc-pVDZ		
(4, 4)	90.5 (85.1)	83.1 (77.7)
(6, 6)/*lp*	86.3 (80.9)	84.9 (79.5)
(10, 10)	86.3 (80.9)	84.3 (78.9)
cc-pVTZ		
(4, 4)	90.9 (85.5)	83.8 (78.4)
(6, 6)/*lp*	86.9 (81.5)	87.4 (82.0)
(10, 10)	86.9 (81.5)	84.8 (79.4)
cc-pVQZ		
(0,0)[a]	100.9 (95.5)	89.9 (84.5)
(4, 4)	90.9 (85.5)	83.7 (78.3)
(6, 6)/*lp*	87.0 (81.6)	87.4 (82.0)
(6, 6)/π	93.4 (88.0)	84.9 (79.5)
(10, 10)	86.9 (81.5)	84.6 (79.2)
(12, 11)	80.8 (75.4)	84.5 (79.1)
Exptl.[b]	79.2 ± 0.8	

[a] MP2 results based on a single reference HF function.
[b] Ref. [8].

$$u_{pq} = (p|h - \delta_{pq}\epsilon_p|q) - \sum_{i}^{\mathrm{doc}} (2g_{pqii} - g_{piiq}) \tag{24}$$

and:

$$\Delta E_{B\alpha} = E_B^{(0)} - E_\alpha^{(0)} \tag{25}$$

as the difference between the energies of the zeroth-order state and configuration. The orbital labels $\{i, j\}$, $\{a\}$, and $\{e\}$ are for doubly occupied, active, and external orbitals, respectively. $\{a', b'\}$ run over both active and external orbitals, and the suffix of the generator $\{p, q, r, s, t, u\}$ runs over only the active orbitals. The terms including doubly occupied orbitals are omitted in this equation. See Ref. [5] for the full formula.

The formula including doubly occupied orbitals might look tedious. However, the energy can be calculated quite easily, as a sum of simple terms. Neither diagonalization nor solution of a linear equation for large-scale matrices is necessary.

The computation is done with the coupling coefficient driven method. These coupling coefficients are sparse and can be pre-screened according to the condition:

$$(v_B^{pq\cdots rs})_{\alpha\beta} = \langle\alpha|E_{pq,\ldots,rs}|B\rangle C_B(\beta) > \delta, \tag{26}$$

where $\delta = 1 \times 10^{-8}$ is usually sufficient to keep the energy accuracy better than 10^{-5} hartree. Thus, the multiple summation for active orbitals in Eqs. (10)–(12), and other terms, which seemingly scales as the power of the number of active orbitals, is actually diminished considerably.

Note that the MRMP energy can also be calculated with Eq. (22) by setting the number of states to one.

1.3. Application of multireference perturbation theory to chemical reaction and excitation spectra

1.3.1. Transition state barrier height for the reaction $H_2CO \rightarrow H_2 + CO$ [7]

The potential energy surface of the reaction $H_2CO \rightarrow H_2 + CO$ has been extensively studied both experimentally and theoretically to clarify the mechanism of the photodissociation process:

$$\begin{array}{c} H_2CO(S_0) \xrightarrow{h\nu} H_2CO(S_1) \\ \qquad\qquad\quad \downarrow \\ \qquad\qquad H_2CO(S_0) \rightarrow H_2 + CO. \end{array}$$

In particular, a precise estimate of the S_0 barrier height of the unimolecular dissociation is important. The experimental study by Polik et al. [8] has confirmed the activation energy of this reaction to be 79.2 ± 0.8 kcal/mol. We present here the results of the second-order multireference Møller–Plesset perturbation theory.

The reaction is Woodward–Hoffmann forbidden and the highly asymmetric transition structure is shown in Fig. 2 of Ref. [9]. We used the geometries determined by CCSD with TZ2p by Scuseria et al. [9]. The basis sets used in the present calculations are Dunning's correlation-consistent basis set: cc-pVDZ, cc-pVTZ, and cc-pVQZ [10]. For the polarization functions of cc-pVQZ, *g* functions on C and O and *f* functions on H were not included.

We employed various choices of CASSCF reference functions to examine a convergent sequence of results. The systematic expansion of CASSCF

reference functions adopted in this study is the following:

CASSCF with (4, 4); {two CH(σ, σ*)}
CASSCF with (6, 6)/π; {two CH(σ, σ*), CO(π, π*)}
CASSCF with (6, 6)/*lp*; {two CH(σ, σ*), O(*lp, lp**)}
CASSCF with (10, 10); {two CH(σ, σ*), O(*lp, lp**), CO(σ, σ*), CO(π, π*)}
CASSCF with (12, 11); {two CH(σ, σ*), O(*lp, lp**), CO(σ, σ*), CO(π, π*), O(2s)}.

The calculated barrier heights are given in Table 1. Values in parentheses include the zero point vibrational energy (ZPVE) correction, and can be directly compared with the experimental estimate of 79.2 ± 0.8 kcal/mol.

The active space is found to have a rather significant effect on the activation energy. The HF results (CAS(0,0)) are poor: the classical barrier (ZPVE corrected value in parentheses) calculated with cc-pVQZ is 100.9 (95.5) kcal/mol, which is about 15 kcal/mol larger than the experimental value. CASSCF represents a great improvement over the HF approximation. CASSCF with a smaller active space such as (4, 4), (6, 6)/*lp*, and (6, 6)/π reduces the HF barrier height by about 10 kcal/mol, although it is still larger than experiment. The computed barrier height decreases with increasing size of the active space.

The MRMP theory corrects the deficiency and represents a great improvement over CASSCF. All barrier heights calculated at the MRMP level are in the range of 83.1 (77.7)–87.4 (82.0) kcal/mol. Even MRMP with relatively small (4, 4) and (6, 6)/π active spaces gives good agreement with experiment. This agreement could be fortuitous due to the overestimation of the dynamical correlation. However, MRMP starting with an adequate zeroth-order CASSCF reference function of (10, 10) and (12, 11) with cc-pVQZ gives almost the same results, 84.6 (79.2) and 84.5 (79.1) kcal/mol. The many-electron wavefunction has almost converged at this level of theory. The agreement of the results with the experimental value, 79.2 ± 0.8 kcal/mol, is also total. Based on these convergence patterns of the one-electron function and the many-electron wavefunction, we conclude that MRMP using the cc-pVQZ basis set and a sufficiently large active space such as (12, 11) and (10, 10) has reached a quantitatively correct description for the barrier height of the reaction.

The quality of the wavefunction calculated at different geometries can be checked by comparison of the weight of the CASSCF reference function in the first-order wavefunction:

$$W = \langle \Psi_{\mathrm{ref}} | \Psi_{\mathrm{ref}} \rangle / \langle \Psi_{\mathrm{ref}} + \Psi^{(1)} | \Psi_{\mathrm{ref}} + \Psi^{(1)} = [1 + \langle \Psi^{(1)} | \Psi^{(1)} \rangle]^{-1}. \quad (27)$$

This weight is a measure for estimating the quality of the perturbed wavefunction. The reference wavefunction has very good quality. Even for the single reference MP2 case, the weight is about 90%, both at the equilibrium and transition state structures. In the case of CASSCF with (10, 10), and (12, 11), the weight is almost 95%, which implies that the second-order perturbation treatment is a good approximation to take account of the rest of the correlation energy.

1.3.2. Excitation spectra of a five-membered compound: furan [11]

Next, we present an application of multireference perturbation theory to the calculation of the excitation spectrum of a five-membered ring compound, furan. Furan and pyrrole are aromatic compounds where the heteroatom supplies two π-electrons and the four carbon atoms supply one π-electron each. These molecules are of importance in synthetic organic chemistry and in biochemistry. Experimental work on the electronic spectrum of these molecules has a long history, but a full characterization is far from complete. The spectrum shows a very complex structure with many overlapping Rydberg series. Knowledge of the location and Franck–Condon profiles of electronic excitations in these molecules is of considerable importance in interpreting results of photochemical experiments.

The calculations were carried out for the ground and low-lying singlet excited states. Experimental geometries were used. The basis sets used for first-row atoms (C and O) are Dunning's cc-pVTZ [10]. The polarization functions were taken from those of cc-pVDZ. The Rydberg functions (2s2p2d) were also placed on the charge center of the molecule. The primitive Rydberg functions for C and O determined

Table 2
Excitation energies and oscillator strengths in furan (eV).

State	Excitation energy							Oscillator strength			
	MRMP[a]	MCQD[a]	Exptl[b]	CASSCF[a]	CASPT2[c]	CC3(CCSD)[d]	SACCI[e]	MRMP	CASPT2[c]	CC3(CCSD)[d]	SACCI[e]
$1^1A_2(1a_2 \rightarrow 3s)$	5.84	5.84	5.91	5.67	5.92	6.11	5.99	0.0	0.0	0.0	0.0
$1^1B_2^+$(Valence)	5.95	5.99	6.06	8.52	6.04	6.35	6.40	1.58×10^{-1}	1.54×10^{-1}	1.44×10^{-1}	1.85×10^{-1}
$2^1A_1^-$(Valence)	6.16	6.19		7.09	6.16	6.61	6.79	3.4×10^{-3}	1.5×10^{-3}	0.000	0.0000
$1^1B_1(1a_2 \rightarrow 3pb_2)$	6.40	6.40	6.48	6.10	6.46	6.64	6.45	1.52×10^{-2}	3.09×10^{-2}	3.5×10^{-2}	3.13×10^{-2}
$2^1B_2(1a_2 \rightarrow 3pb_1)$	6.50	6.51	6.48	6.42	6.48	6.94	6.82	2.66×10^{-2}	4.71×10^{-2}	1.5×10^{-5}	1.58×10^{-2}
$2^1A_2(1a_2 \rightarrow 3pa_1)$	6.53	6.54	6.61	6.20	6.59	6.80	6.66	0.0	0.0	0.0	0.0
$3^1A_2(1a_2 \rightarrow 3da_1)$	6.98	6.98		6.64	7.00	7.12	7.04	0.0	0.0	0.0	0.0
$2^1B_1(1a_2 \rightarrow 3db_2)$	7.10	7.12		6.71	7.15	7.32	7.14	3.71×10^{-5}	0.0000	$1.\times10^{-3}$	$5.\times10^{-4}$
$4^1A_2(1a_2 \rightarrow 3da_1)$	7.18	7.19		6.77	7.22	7.12	7.72	0.0	0.0	0.0	0.0
$3^1B_2(1a_2 \rightarrow 3db_1)$	7.18	7.21		7.05	7.13	7.72	7.51	1.03×10^{-2}	7.4×10^{-3}	1.6×10^{-2}	1.94×10^{-2}
$3^1A_1(1a_2 \rightarrow 3da_2)$	7.26	7.29	7.28	7.34	7.31	7.58	7.36	7.29×10^{-5}	$3.\times10^{-4}$	0.000	$1.\times10^{-4}$
$3^1B_1(2b_1 \rightarrow 3s)$	7.31	7.25	7.38	6.81	7.21	7.52	7.45	1.49×10^{-2}	1.92×10^{-2}	2.2×10^{-2}	2.92×10^{-2}
$4^1A_1^+$(Valence)	7.69	7.72	7.82	10.51	7.74	8.35	8.34	4.94×10^{-1}	4.16×10^{-1}	3.50×10^{-1}	4.83×10^{-1}

[a] The ground state energy is −229.390926 au (MRMP), −229.390926 au (MCQD), and −228.714660 au (CASSCF).
[b] See references in Ref. [11].
[c] Ref. [13].
[d] Ref. [14].
[e] Ref. [15].

by Dunning and Hay [12] were weight-averaged and split into two with splitting factors of 1.9 and 0.75. The cc-pVDZ was used for hydrogen atoms (no polarization on H). We first carried out the state-averaged CASSCF calculations in each symmetry and then performed perturbation calculations with MRMP PT and MC-QDPT.

Calculated vertical excitation energies and oscillator strengths, along with the available experimental data, are summarized in Table 2. The results of the CASSCF plus second-order perturbation theory (CASPT2) by Serrano-Andres et al. [13], the coupled cluster method (CC3 and CCSD) by Christiansen and Jørgensen [14], and the CI calculation based on the symmetry-adapted cluster expansion method (SAC-CI) by Wan et al. [15] and are also listed in Table 2.

First, we will discuss the valence excited states. The first band in the absorption spectrum appears at 6.06 eV [16,17]. Flicker et al. [18,19] assigned the optically allowed transition at 6.06 eV as the $^1A_1 \rightarrow {}^1B_2$ excitation from the study of electron impact spectroscopy. Theory shows that the $^1B_2^+$ state is the lowest valence state of ionic nature. MRMP predicts that the $^1B_2^+$ state lies at 5.95 eV and MCQD at 5.99 eV, respectively. This state is well represented by a single $\pi \rightarrow \pi^*$ excitation. The oscillator strength is computed to be 0.158, which is to be compared with the experimental value of 0.12 [17]. The second valence excited state is $2^1A_1^-$. Transition to the A_1^- state is pseudoparity forbidden and, thus, there is no experimental evidence of this transition. MRMP predicts that the $2^1A_1^-$ state lies at 6.16 eV and MCQD at 6.19 eV with weak intensity. The most intense feature of the absorption spectrum, with a maximum at 7.79 eV [16], is due to the transition to the third valence excited state, $4^1A_1^+$. The electron impact investigation located the state at 7.82 eV [19]. MRMP placed the $4^1A_1^+$ state at 7.69 eV and MCQD at 7.72 eV with a high intensity of 0.494.

Next, let us discuss the Rydberg transitions. The first singlet–singlet excitation of furan is the 3s-Rydberg series. Robin [20] assigned the weak peak at 5.94 eV to the dipole-forbidden $^1A_2$ Rydberg transition. Roebber et al. [21] also assigned the peak at 5.91 eV to the $1a_2 \rightarrow 3s$ Rydberg state using multiphoton ionization spectroscopy. The computed excitation energy is 5.84 eV. The second band system observed in the absorption spectrum of furan shows sharp bands that could be analyzed to reveal vibrational frequencies of the excited molecule [16]. The computed $3p^1B_1$ transition energy is 6.40 eV, which is in good agreement with experiment [22,23]. Theory predicts that another dipole-allowed 3p-Rydberg state, $^1B_2$, lies above $^1B_1$. The dipole-forbidden 3p-Rydberg transition to $^1A_2$ has not been observed explicitly, but theory predicts that the state exists around 6.54 eV, slightly above the $3p^1B_2$ and $3p^1B_1$ states. The states following the three 3p-Rydberg states are five 3d-Rydberg states. Present theory predicts five states lying in the range of 6.98–7.29 eV with low intensities, except for 3^1B_2 (the oscillator strength of the transition to 3^1B_2 is computed to be 0.0103). The 3^1A_1 state is predicted to lie at 7.26 eV (MRMP) and at 7.29 eV (MCQD) with very weak intensity. A band at 7.39 eV with high intensity among the third band system of the absorption spectrum was first observed by Pickett [16]. The calculated $2b_1 \rightarrow 3s$ transition energies are 7.31 eV (MRMP) and 7.25 eV (MCQD). The transition is predicted to have a relatively high intensity of 0.015.

On the whole, the present approach leads to the prediction of the spectrum of the molecule that provides a consistent assignment of the experimental data.

1.4. QCAS-SCF method and QCAS-QDPT—extension of reference wavefunction

1.4.1. Quasi-complete active space self-consistent field (QCAS-SCF) method [24]

In the study of chemical reaction mechanisms, the multiconfiguration self-consistent field (MCSCF) method is a very useful approach and, hence, frequently used, especially in the form of the complete active space self-consistent field (CASSCF) method. However, CASSCF often generates far too many configurations, and the size of the active space outgrows the capacity of present technology. Even today, the size of the configuration interaction (CI) space that can be routinely used has a dimension of about one million at most, which roughly corresponds to 12–14 active orbitals.

We have proposed an MCSCF method with a quasi-complete active space (QCAS), i.e. a QCAS-SCF method. In the MCSCF method, we partition orbitals into core, active, and virtual, then construct the CI

Table 3
Bond length, vibrational frequency, and dissociation energy for CO molecule

	Dimension	r_e (Å)	ω_e (cm^{-1})	D_e (kcal/mol)
CAS(12, 12)	48,200	1.1325	2175	247.2
QCAS[(4, 4)^3]	4096	1.1324	2175	248.0
Exptl.[a]		1.128323	2169.8	255.8

[a] Ref. [25].

space by distributing active electrons among the active orbitals. Let us further divide the active electron and orbital sets into N sub-sets and fix the number of active electrons, m_i, and orbitals, n_i, in each sub-set:

$$m_{\mathrm{act}} = \sum_i^N m_i, n_{\mathrm{act}} = \sum_i^N n_i, \tag{28}$$

where m_{act} and n_{act} denote the number of active electrons and orbitals, respectively. We define the quasi-complete space as the product space of CAS spanned by the determinants or CSF as follows:

$$\mathrm{QCAS}(\{m_i\},\{n_i\}) = \mathrm{CAS}(m_1,n_1)\times\mathrm{CAS}(m_2,n_2) \times\cdots\times\mathrm{CAS}(m_N,n_N) \tag{29}$$

such that the number of electrons in each orbital group satisfies the restriction in Eq. (28).

The dimension of QCAS can be much smaller than that of CAS for the same set of active electrons and orbitals. For example, the dimension of CAS(16, 16) spanned by the determinants with $M=0$ is 165,636,900 (the dimension of an active space is expressed by the number of determinants with $M=0$ and no symmetry). If we divide the active electrons and orbitals into five groups, (4e, 4o) + (4e, 4o) + (4e, 4o) + (2e, 2o) + (2e, 2o), where 4e and 4o denote four electrons and four orbitals in the group, respectively, the dimension of QCAS is 746,496 ($=36^3\times4^2$).

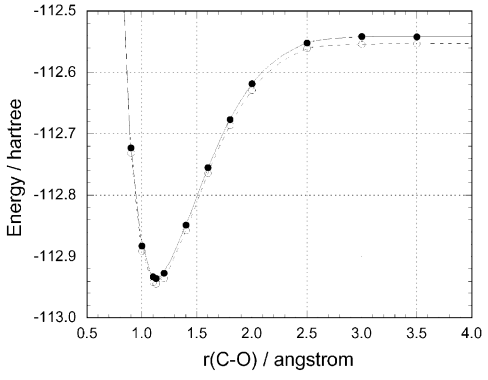

Fig. 1. The QCAS-SCF (●) and CAS-SCF (○) potential curves of the ground state ($X^1\Sigma^+$) of CO.

The efficiency of the MCSCF optimization can be improved by the use of Slater determinants. We further split a determinant into an alpha and beta string of each group:

$$|I\rangle = |I_\alpha^1\cdots I_\alpha^N; I_\beta^1\cdots I_\beta^N\rangle = |I_\alpha^1\rangle\cdots|I_\alpha^N\rangle|I_\beta^1|\rangle\cdots|I_\beta^N\rangle, \tag{30}$$

where $|I\rangle$ are now determinants and $|I_\alpha^G\rangle$ and $|I_\beta^G\rangle$ are segmented alpha and beta strings of group G, respectively. The characteristic feature to be noted is that, if we use the determinants in Eq. (30), both the σ-vector and density formulas are written only with one-electron coupling constants between *strings in a group,* and no intergroup coupling constants appear. This fact makes the QCAS-CI eigenvector computation very efficient. Note that by using CSF we cannot reach a similar decoupling.

We have calculated some spectroscopic constants and a potential energy curve of CO with QCAS-SCF, and compared the results with those of CASSCF with corresponding active spaces. The basis set used is the cc-pVTZ basis set of Dunning [10]. The active spaces were constructed from six electrons and 12 (5σ–8σ, 1π–4π, and $1\pi'$–$4\pi'$) orbitals. CAS was used for comparison and was constructed by distributing these six electrons among all 12 orbitals. QCAS was constructed by first dividing the orbitals into three groups, $\{5\sigma$–$8\sigma\}$, $\{1\pi$–$4\pi\}$, and $\{1\pi'$–$4\pi'\}$, and then distributing two electrons among each group. Henceforth, we call this active space QCAS[(2, 4)^3]. The dimension of QCAS[(2, 4)^3] is 4096, while that of CAS(6, 12) is 48,200.

Table 3 summarizes the results for some spectroscopic constants. All the constants, r_e, ω_e, and D_e, of

QCAS-SCF are in very good agreement with those of CASSCF. The differences from CASSCF in r_e and ω_e are less than 0.001 Å and 1 cm^{-1}, respectively, and that in D_e is only 0.8 kcal/mol. Fig. 1 shows the potential curves of the ground state, $X^1\Sigma^+$, calculated with the QCAS-SCF and CASSCF methods. Although the QCAS-SCF curve is about 10 millihartree above the CASSCF curve, QCAS-SCF reproduces the shape of the CASSCF potential curve very well. The difference is almost constant (maximum deviation in energy difference is about 5 millihartree) for the entire bond length. It is the shape of a potential curve that is important in chemical reaction studies, not the absolute energy. Thus, it can be said that QCAS-SCF exhibits high performance.

1.4.2. Quasi-degenerate perturbation theory with quasi-complete active space self-consistent field reference functions (QCAS-QDPT) [26]

So far, the implementation of these MRPTs is only for the CASSCF reference functions. The dimension of the CAS grows very rapidly as the number of active orbitals increases, which sometimes makes implementation of a perturbation computation impossible. Perturbation methods using a selected reference configuration space, but retaining the advantages of the CAS based PTs, are necessary. Combining QCAS with MC-QDPT provides an effective tool for electronic structure theory. We present MC-QDPT using QCAS-SCF reference functions. (Hereafter, we call it QCAS-QDPT, while we call MC-QDPT with CAS reference CAS-QDPT.)

Adopting (state-averaged) QCAS-SCF wavefunctions α (β) as reference functions that define P space, we obtain the effective Hamiltonian to the second order:

$$(K_{\mathrm{eff}}^{(0-2)})_{\alpha\beta} = E_\alpha^{\mathrm{QCAS}}\delta_{\alpha\beta} + \frac{1}{2}\left\{\sum_{I\notin \mathrm{QCAS}} \frac{\langle\alpha|V|I\rangle\langle I|V|\beta\rangle}{E_\beta^{(0)} - E_I^{(0)}} + (\alpha \leftrightarrow \beta)\right\}, \tag{31}$$

which corresponds to Eq. (21) in the CASSCF reference case. Let us define a *corresponding complete active space* (CCAS) to a QCAS as the complete active space that has the same active orbital set and electron set but does not have the limitation, Eq. (28). In other words, the corresponding CAS is the minimal CAS that includes the QCAS. Then the summation for I in Eq. (31) may be divided into the summations for determinants/CSFs outside the CAS and for the determinants/CSFs outside the QCAS, but inside the corresponding CAS:

$$\sum_{I\notin \mathrm{QCAS}} = \sum_{I\notin \mathrm{CCAS}} + \sum_{I\in \mathrm{CCAS}\wedge I\notin \mathrm{QCAS}}, \tag{32}$$

and then the first second-order term in Eq. (31) may be written as:

$$(K_{\mathrm{eff}}^{(2)})_{\alpha\beta} = \sum_{I\notin \mathrm{CCAS}} \frac{\langle\alpha|V|I\rangle\langle I|V|\beta\rangle}{E_\beta^{(0)} - E_I^{(0)}} + \sum_{I\in \mathrm{CCAS}\wedge I\notin \mathrm{QCAS}} \frac{\langle\alpha|V|I\rangle\langle I|V|\beta\rangle}{E_\beta^{(0)} - E_I^{(0)}}. \tag{33}$$

The first term in Eq. (33) involves excitations from core orbitals and excitations to virtual orbitals in the intermediate states I (the *external* terms), while the second term involves excitations where only active orbitals are involved (the *internal* terms). The second-order effective Hamiltonian (33) is expressed by 25 external term and nine internal term diagrams. Since QCAS is a natural extension of CAS, computation of these diagrams can be done efficiently in a similar manner to CAS-QDPT.

The ground state and triplet and singlet Rydberg excited states of furan were calculated as an example. The geometry and basis set used are the same as those in Section 1.3.2. We carried out the nine-state-averaged QCAS-SCF calculations for all 3s, 3p, and 3d Rydberg states. The active orbital set consists of five valence π and π^* orbitals and nine Rydberg orbitals. This orbital set was divided into two groups, five valence orbitals and nine Rydberg orbitals. For triplet Rydberg states, QCAS was constructed by distributing five electrons (three alpha and two beta electrons) to five valence orbitals and one alpha electron to nine Rydberg orbitals, QCAS[$(3\alpha 2\beta, 5)\times(1\alpha, 9)$]. For singlet Rydberg states, the active space was constructed from the QCASs that were made in a similar way to the triplet case, QCAS[$(3\alpha 2\beta, 5)\times(1\beta, 9)$] and QCAS[$(2\alpha 3\beta, 5)\times(1\alpha, 9)$]. Since both of them are necessary for the active space to take into account proper spin-coupling, we use their direct sum, QCAS[$(3\alpha\, 2\beta, 5)\times(1\beta, 9) + (2\alpha\, 3\beta, 5)\times(1\alpha, 9)$]. These QCASs are applicable to the single excitations from a π valence orbital to a 3spd Rydberg orbital. The dimensions of the triplet and singlet QCASs

Table 4
Rydberg excitation energies of furan (eV)

State	Singlet					Triplet			
	QCAS-SCF	QCAS-QDPT	CAS-SCF[a]	CAS-QDPT[a]	Exptl.[b]	QCAS-SCF	QCAS-QDPT	CAS-SCF	CAS-QDPT
$A_2(1a_2 \rightarrow 3s)$	5.62	5.84	5.67	5.84	5.91	5.56	5.76	5.61	5.78
$B_1(1a_2 \rightarrow 3pb_2)$	6.03	6.37	6.10	6.40	6.48	5.99	6.31	6.08	6.37
$B_2(1a_2 \rightarrow 3pb_1)$	6.21	6.41	6.42	6.51	6.48	6.16	6.49	6.34	6.57
$A_2(1a_2 \rightarrow 3pa_1)$	6.19	6.53	6.20	6.54	6.61	6.18	6.50	6.19	6.52
$A_2(1a_2 \rightarrow 3da_1)$	6.61	6.96	6.64	6.98	–	6.55	6.86	6.58	6.88
$B_1(1a_2 \rightarrow 3db_2)$	6.69	7.09	6.71	7.12	–	6.67	7.05	6.69	7.09
$A_2(1a_2 \rightarrow 3da_1)$	6.77	7.19	6.77	7.19	–	6.75	7.15	6.75	7.16
$B_2(1a_2 \rightarrow 3db_1)$	6.87	7.10	7.05	7.21	–	6.87	7.16	7.06	7.40
$A_1(1a_2 \rightarrow 3da_2)$	6.82	7.30	7.34	7.29	7.28	6.77	7.23	7.11	7.28

[a] Ref. [35].
[b] See references in Ref. [35].

are 900 and 1800, respectively. For the ground state, we used QCAS[(6, 5) × (0, 9)], which is equivalent to CAS(6, 5).

Perturbation calculations were performed for the nine triplet and nine singlet 3spd Rydberg states and the ground state. The results are summarized in Table 4, as well as the experimental and previous results. Singlet QCAS-SCF results are in good agreement with the CASSCF results (<0.1 eV) except for the 3p $^1B_2$, 3d $^1B_2$, and 3d $^1A_1$ Rydberg states. For these states, the CASSCF values are 0.21 (3p $^1B_2$), 0.18 (3d $^1B_2$), and 0.52 eV (3d $^1A_1$) higher than the QCAS-SCF values, since the CASSCF optimizations also included valence states of the same symmetry. On the other hand, the QCAS-QDPT results are very close to the CAS-QDPT results in all the states. The average and maximum differences are only 0.03 and 0.11 eV, respectively. Moreover, the QCAS-QDPT excitation energies also reproduce the available experimental results well. The error is at most 0.11 eV. Most triplet states are slightly lower than the corresponding singlet states (by 0.8 eV at maximum) in both the reference and QCAS-QDPT levels. Also, in the triplet states the QCAS-QDPT results are very close to the CAS-QDPT results, except for the 3d $^3B_2$ state. The average and maximum differences are only 0.06 and 0.24 eV, respectively.

1.4.3. Energy gradient of multireference perturbation theory [27,28]

The analytic energy derivative method is an essential technique in modern electronic structure theory. Geometry optimization is a key step in studying chemical reaction mechanisms and molecular structures, and normal mode vibrational analysis is utilized to predict infrared and Raman spectra. The required information is obtained from the first and second derivatives with respect to nuclear coordinates of a molecule. A derivation of the analytic gradients for second-order MC-QDPT is done from a basis of the response function formalism [29,30].

The Lagrangian is defined by:

$$L(X, \zeta, C) = W(X, C) + \zeta e(X, C) \tag{34}$$

where X is a nuclear coordinate, C represents the molecular orbital, configuration interaction coefficients of the reference functions and other parameters, W is the energy, e represents constraints on the parameters C, and ζ is the Lagrangian multiplier. The energy expression W is given by:

$$W = \sum_{\alpha\beta} D_\alpha D_\beta (K_{\text{eff}}^{(0-2)})_{\alpha\beta}, \tag{35}$$

where D_a is the element of the eigenvector of the effective Hamiltonian, and the constraints $e(X,C)$ are (i) the (state-averaged) CASSCF equation, (ii) the orbital canonicalization condition, (iii) the orthonormalization condition of the orbitals, (iv) the diagonalization condition of the effective Hamiltonian, and some auxiliary conditions.

The parameters ζ are determined such that the first derivative of the Lagrangian with respect to the Cs is

zero:

$$\frac{\partial L}{\partial C} = \frac{\partial L}{\partial C} + \zeta \frac{\partial e}{\partial C} = 0. \quad (36)$$

Using the parameter determined by Eq. (36), the molecular gradients are simply given by:

$$\frac{\partial L}{\partial X} = \frac{\partial}{\partial X}(W + \zeta e). \quad (37)$$

The explicit expressions of Eqs. (36) and (37) are actually very long. See Refs. [27,28] for details.

2. Valence bond description of complete active space self-consistent field function

A defect of the multireference-based methods is that the wavefunction is too complicated to extract a chemical description from it. There are too many CI coefficients, cluster amplitudes, or terms corresponding to diagrams in those methods. The information of the chemical picture is hidden behind them and to extract it seems quite difficult.

The classical valence bond (VB) theory is very successful in providing qualitative explanation for many aspects. Chemists are familiar with the localized molecular orbitals (LMO) and the classical VB resonance concepts. If modern accurate wavefunctions can be represented in terms of such well-known concepts, chemists' intuition and experiences will give a firm theoretical basis and the role of computational chemistry will undoubtedly expand. In the CASVB method, reference CASSCF wavefunctions are transformed into valence bond functions without any loss of CASSCF quality.

2.1. CASVB method [31,32]

We have proposed two different CASVB methods [31,32]. In one method, the valence bond structures are constructed over *orthogonal* localized orbitals; in the other method, the structures are written with *non-orthogonal* localized orbitals. These are henceforth referred to as orthogonal CASVB and non-orthogonal CASVB, respectively.

The idea of CASVB is based on the fact that the densities of variational wavefunctions are invariant under the transformations that hold the variational space unchanged. In the CASSCF case, a complete active space (CAS) is invariant under the linear transformation of active orbitals and also that of configuration state functions (CSFs).

One may redefine the active orbitals utilizing the invariance of the active orbital space. In the orthogonal CASVB method, the localized molecular orbitals (LMOs) constructed by Boys' localization procedure are used; that is, active orbitals are transformed so as to have the minimum sum of r^2 expectation values [33]. If the active orbitals are defined appropriately, the LMOs obtained nearly always turn out to be localized on a single atomic center with small localization tails onto neighboring atoms. In the non-orthogonal CASVB case, the atomic-like orbitals are constructed by Ruedenberg's projected localization procedure [34–36].

Let Ψ^{CASSCF} be a CASSCF wavefunction:

$$\Psi^{\mathrm{CASSCF}} = \sum_i C_i \Phi_i^{\mathrm{CSF}}, \Phi_i^{\mathrm{CSF}} \equiv \Phi_i^{\mathrm{CSF}}(\{\varphi_i\}), \quad (38)$$

where Φ_i^{CSF} are the configuration state functions constructed by the orthogonal orbitals set $\{\varphi_i\}$ and C_i are the known CAS configuration interaction expansion coefficients. Similarly, one may define the CASVB function in terms of spin-paired functions as:

$$\Psi^{\mathrm{CASVB}} = \sum_i A_i \Phi_i^{\mathrm{VB}}, \Phi_i^{\mathrm{VB}} \equiv \Phi_i^{\mathrm{VB}}(\{\lambda_i\}), \quad (39)$$

where Φ_i^{VB} is a spin-paired function constructed by LMOs. The spaces, spanned by $\{\Phi_i^{\mathrm{CSF}}\}$ and $\{\Phi_i^{\mathrm{VB}}\}$, are identical. Since Eqs. (38) and (39) are different expressions of the identical wavefunction, one may write:

$$\sum_j A_j \Phi_j^{\mathrm{VB}} = \sum_j C_j \Phi_j^{\mathrm{CSF}}. \quad (40)$$

Multiplying Eqs. (38) and (39) by Φ_i^{CSF} and integrating the products, one has a linear equation:

$$\sum_j \Omega_{ij} A_j = C_i \text{ wtih } \Omega_{ij} = \langle \Phi_i^{\mathrm{CSF}} | \Phi_j^{\mathrm{VB}} \rangle, \quad (41)$$

which has a dimension equal to the dimension of the CAS. Solving this linear equation, one obtains the CASVB wavefunction Ψ^{CASVB}. In the orthogonal CASVB case, one can use the common set of (Boys') LMOs as $\{\varphi_i\}$ as well as $\{\lambda_i\}$, since the LMOs remain CASSCF MOs. In that case, the linear equation (41) is reduced to a set of linear equations for

Table 5
The occupation numbers of the ground and excited state CASVB wavefunctions of butadiene

Structure	Occupation numbers	
	Orthogonal MO	Non-orthogonal MO
$1^1A_g^-$ (ground state)		
[C=C–C=C]	0.3960	0.4789
[$\overline{\text{C–C=C–C}}$]	0.0525	0.0633
[$C^- - C^+ - C{=}C$] + [$C{=}C{-}C^+ - C^-$]	0.1970	0.1746
[$C^+ - C^- - C{=}C$] + [$C{=}C{-}C^- - C^+$]	0.1812	0.1565
[$\overline{\text{C–C}^+ - \text{C}^- - \text{C}}$] + [$\overline{\text{C–C}^- - \text{C}^+ - \text{C}}$]	0.0436	0.0312
[$C^- - \overline{\text{C–C}^+ - \text{C}}$] + [$\overline{\text{C–C}^- - \text{C}}$–$C^+$]	0.0194	0.0185
[$C^+ - \overline{\text{C–C}^- - \text{C}}$] + [$\overline{\text{C–C}^- - \text{C}}$–$C^+$]	0.0152	0.0126
[$C^- - C{=}C{-}C^+$] + [$C^+ - C{=}C{-}C^-$]	0.0102	0.0102
[$C^- - C^+ - C^- - C^+$] + [$C^+ - C^- - C^+ - C^-$]	0.0506	0.0369
[$C^- - C^+ - C^+ - C^-$]	0.0182	0.0100
[$C^+ - C^- - C^- - C^+$]	0.0155	0.0078
[$C^- - C^- - C^+ - C^+$] + [$C^+ - C^+ - C^- - C^-$]	0.0002	− 0.0002
$2^1A_g^-$ (covalent)		
[$\overline{\text{C–C=C–C}}$]	0.6059	0.6439
[C=C–C=C]	0.0789	0.0809
[$\overline{\text{C–C}^+ - \text{C}^- - \text{C}}$] + [$\overline{\text{C–C}^- - \text{C}^+ - \text{C}}$]	0.2330	0.1967
[$C^+ - \overline{\text{C–C}^- - \text{C}}$] + [$\overline{\text{C–C}^- - \text{C}}$–$C^+$]	0.0219	0.0249
[$C^- - \overline{\text{C–C}^+ - \text{C}}$] + [$\overline{\text{C–C}^- - \text{C}}$–$C^+$]	0.0118	0.0166
[$C^- - C^+ - C{=}C$] + [$C{=}C{-}C^+ - C^-$]	0.0188	0.0169
[$C^+ - C^- - C{=}C$] + [$C{=}C{-}C^- - C^+$]	0.0154	0.0142
[$C^- - C{=}C{-}C^+$] + [$C^+ - C{=}C{-}C^-$]	0.0040	0.0040
[$C^+ - C^- - C^- - C^+$]	0.0037	0.0026
[$C^- - C^+ - C^+ - C^-$]	0.0028	0.0017
[$C^- - C^+ - C^- - C^+$] + [$C^+ - C^- - C^+ - C^-$]	0.0038	0.0024
[$C^- - C^- - C^+ - C^+$] + [$C^+ - C^+ - C^- - C^-$]	0.0002	0.0000
$1^1B_u^+$ (ionic)		
[$C^- - C^+ - C{=}C$] − [$C{=}C{-}C^+ - C^-$]	0.1940	0.2157
[$C^+ - C^- - C{=}C$] − [$C{=}C{-}C^- - C^+$]	0.1488	0.1655
[$C^- - C{=}C{-}C^+$] − [$C^+ - C{=}C{-}C^-$]	0.1362	0.1367
[$C^- - \overline{\text{C–C}^+ - \text{C}}$] − [$\overline{\text{C–C}^- - \text{C}}$–$C^+$]	0.1322	0.1278
[$C^+ - \overline{\text{C–C}^- - \text{C}}$] − [$\overline{\text{C–C}^- - \text{C}}$–$C^+$]	0.1006	0.0942
[$\overline{\text{C–C}^+ - \text{C}^- - \text{C}}$] − [$\overline{\text{C–C}^- - \text{C}^+ - \text{C}}$]	0.0948	0.1038
[$C^- - C^+ - C^- - C^+$] − [$C^+ - C^- - C^+ - C^-$]	0.1900	0.1576
[$C^- - C^- - C^+ - C^+$] − [$C^+ - C^+ - C^- - C^-$]	0.0034	− 0.0014

each *orbital* configuration, and the matrix Ω_{ij} for each linear equation becomes a triangular matrix depending only on spin configurations. The linear equation (41) can, therefore, be solved with ease, compared with the non-orthogonal CASVB case.

The occupation number (or weight) of a resonance structure is calculated with:

$$n_i = A_i^* \sum_j S_{ij} A_j, \tag{42}$$

where S_{ij} are overlap integrals between the structures i and j, defined by:

$$S_{ij} = \langle \Phi_i^{\mathrm{VB}} | \Phi_j^{\mathrm{VB}} \rangle. \tag{43}$$

and satisfies the normalization:

$$\sum_i n_i = 1. \tag{44}$$

Note that the occupation number n_i could be negative because of the non-orthogonality of resonance structures.

2.2. Description of electronic structure

Butadiene is a good molecule to show the usefulness of CASVB. CASSCF functions were computed with an active space of four π-electrons in four π-orbitals. The calculations were performed using the experimental geometry with the (3s2pld/2s) basis. Both the orthogonal and non-orthogonal π LMOs of *trans*-butadiene were used. The π LMOs are well localized on a single atomic center with small localization tails onto the neighboring carbons. Each π LMO resembles an atomic-like 2p function. The overlap between the terminal (center) π LMO and an atomic 2p of the free atom is 0.9912 (0.9883).

The occupation numbers for *trans*-butadiene are summarized in Table 5. The ground state is of covalent nature and mainly comprised of the Kekule-type structure:

[C=C–C=C]

with a small contribution from the Dewar-type structure:

[$\overline{\text{C–C=C–C}}$].

The $2\,^1A_g^-$ state is also of covalent nature. In an MO treatment, the state is described by a significant contribution from the singly excited configurations of (HOMO) → (LUMO + 1) and (HOMO − 1) → (LUMO), and the doubly excited configuration of $(\mathrm{HOMO})^2 \rightarrow (\mathrm{LUMO})^2$. In the CASVB treatment, this state is expressed predominantly by a Dewar-type structure with small mixing from the Kekule-type structure. We can see from Table 5 that CASVB with non-orthogonal orbitals makes the weights of the covalent structures increase relative to those of the ionic structures in both covalent states. The dipole-allowed $1\,^1B_u^+$ state is well described by a singly excited configuration, (HOMO) → (LUMO) in an MO description. The state has an ionic nature that can be readily interpreted in terms of the VB resonance structures. The $1\,^1B_u^+$ state is a mixture of a large number of ionic structures. The covalent structures are strictly excluded from the ionic states. The leading terms are the singly and doubly polar structures, for example:

$[C^-–C^+–C=C]–[C=C–C^+–C^-]$

and:

$[C^-–C^+–C^-–C^+]–[C^+–C^-–C^+–C^-]$.

Although singly and doubly ionic structures have nearly the same occupation numbers when orthogonal orbitals are used, use of non-orthogonal orbitals enhances the weight of singly ionic structures and diminishes the weight of more polar doubly ionic structures.

2.3. Description of chemical reaction [37]

We present the application of CASVB to chemical reactions. The main purpose is to propose a quantitative measure of the chemical picture at the transition state (TS) and along the chemical reaction paths.

The example used here is the dissociation reaction of formaldehyde into a hydrogen molecule and carbon monoxide. A qualitatively correct description of the dissociation process requires at least four active electrons in the two CH bonds of H_2CO. During the dissociation process, two electrons, one from each CH bond, pair up to form the HH bond while the other two form a lone pair on C in CO. The dominant non-dynamical correlation of the reaction is described by a CASSCF wavefunction including all configurations generated by distributing these four electrons in four

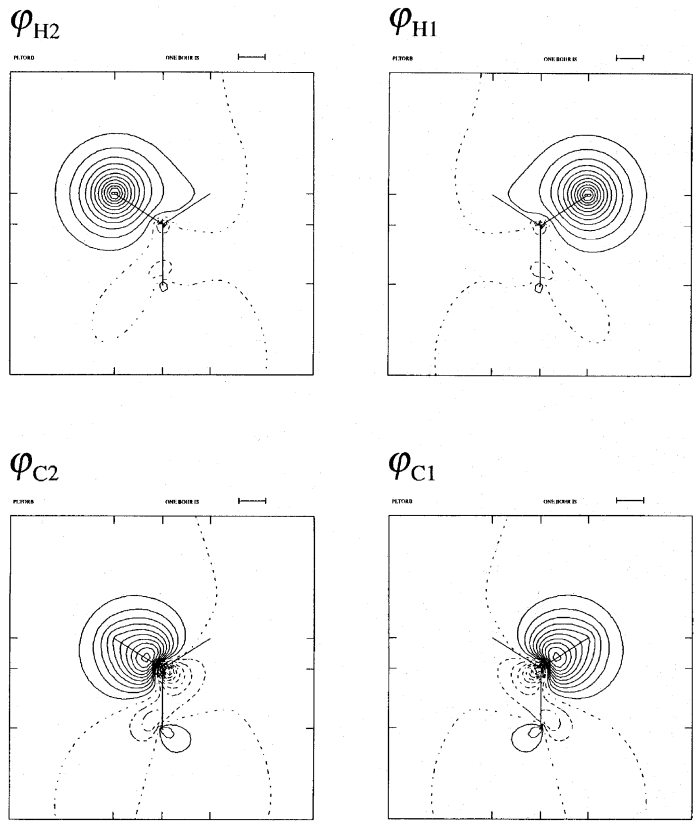

Fig. 2. The non-orthogonal localized orbitals at the equilibrium structure of H_2CO determined with Ruedenberg's projected localization procedure.

active orbitals, two CH bonding and antibonding pairs.

The CASSCF wavefunction was obtained with CAS(4, 4). The basis set used was Dunning's correlation-consistent valence double zeta plus polarization basis set (cc-pVDZ) [10]. The equilibrium structure and the transition state were determined by these calculations.

There are 20 linearly independent spin-paired functions corresponding to the dimension of CAS(4, 4):

$$\varphi_{C1}\varphi_{H1}(\alpha\beta-\beta\alpha)\cdot\varphi_{H2}\varphi_{C2}(\alpha\beta-\beta\alpha), \quad \text{(I)}$$

$$\varphi_{C1}\varphi_{H1}(\alpha\beta-\beta\alpha)\cdot\varphi_{H2}\varphi_{H2}\alpha\beta, \quad \text{(II)}$$

$$\varphi_{C1}\varphi_{H1}(\alpha\beta-\beta\alpha)\cdot\varphi_{C2}\varphi_{C2}\alpha\beta, \quad \text{(III)}$$

$$\varphi_{C1}\varphi_{C1}\alpha\beta\cdot\varphi_{H2}\varphi_{C2}(\alpha\beta-\beta\alpha), \quad \text{(IV)}$$

$$\varphi_{H1}\varphi_{H1}\alpha\beta\cdot\varphi_{H2}\varphi_{C2}(\alpha\beta-\beta\alpha), \quad \text{(V)}$$

$$\varphi_{C1}\varphi_{H2}(\alpha\beta-\beta\alpha)\cdot\varphi_{H1}\varphi_{H1}\alpha\beta, \quad \text{(VI)}$$

$$\varphi_{C1}\varphi_{H2}(\alpha\beta-\beta\alpha)\cdot\varphi_{C2}\varphi_{C2}\alpha\beta, \quad \text{(VII)}$$

$$\varphi_{C2}\varphi_{H1}(\alpha\beta-\beta\alpha)\cdot\varphi_{C1}\varphi_{C1}\alpha\beta, \quad \text{(VIII)}$$

$$\varphi_{C2}\varphi_{H1}(\alpha\beta-\beta\alpha)\cdot\varphi_{H2}\varphi_{H2}\alpha\beta, \quad \text{(IX)}$$

$$\varphi_{C1}\varphi_{C2}(\alpha\beta-\beta\alpha)\cdot\varphi_{H1}\varphi_{H2}(\alpha\beta-\beta\alpha), \quad \text{(X)}$$

$$\varphi_{C1}\varphi_{C1}\alpha\beta\cdot\varphi_{H1}\varphi_{H2}(\alpha\beta-\beta\alpha), \quad \text{(XI)}$$

$$\varphi_{C2}\varphi_{C2}\alpha\beta\cdot\varphi_{H1}\varphi_{H2}(\alpha\beta-\beta\alpha), \quad \text{(XII)}$$

$$\varphi_{C1}\varphi_{C2}(\alpha\beta-\beta\alpha)\cdot\varphi_{H1}\varphi_{H1}\alpha\beta, \quad \text{(XIII)}$$

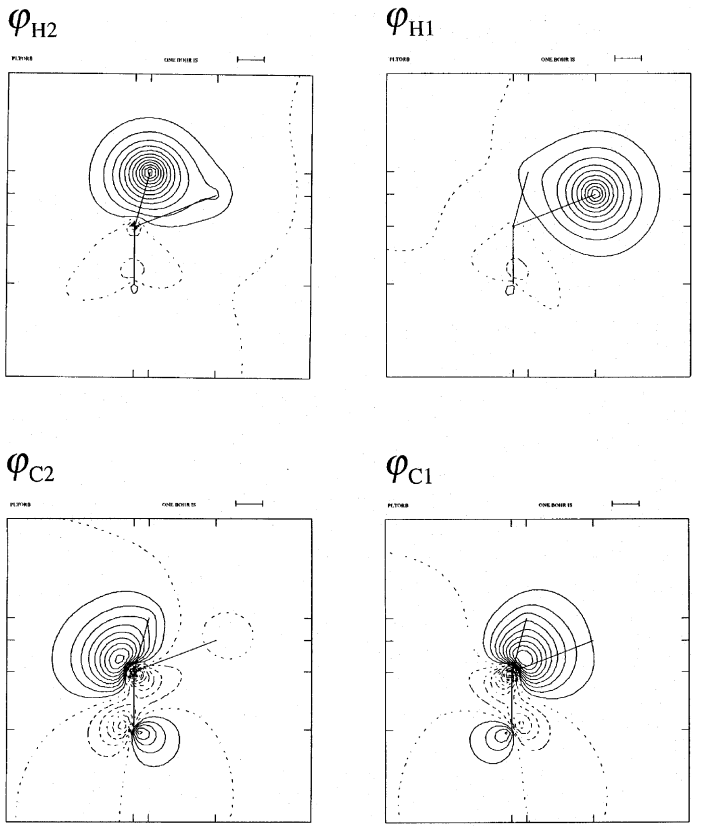

Fig. 3. The non-orthogonal localized orbitals at the transition state structure of the $H_2CO \rightarrow H_2 + CO$ reaction.

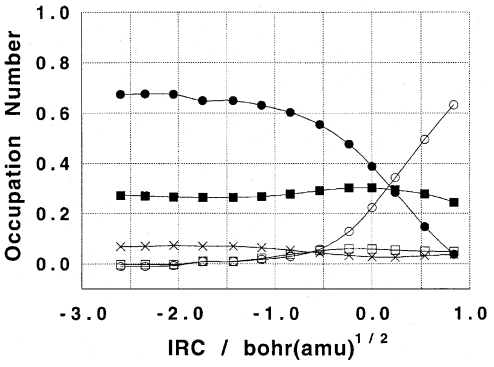

Fig. 4. Changes in the occupation numbers of the covalent CH bonds (●), ionic CH bonds (■), covalent HH bond (○), ionic HH bond (□), and the other (doubly ionic) (×) VB structures of H_2CO along IRC.

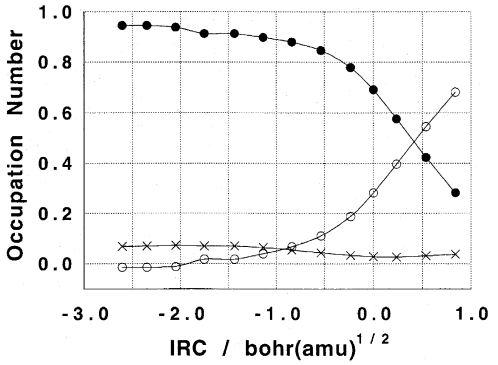

Fig. 5. Changes in the occupation numbers of the total CH bonds (●), total HH bond (○), and the other (doubly ionic) (×) VB structures of H_2CO along the IRC.

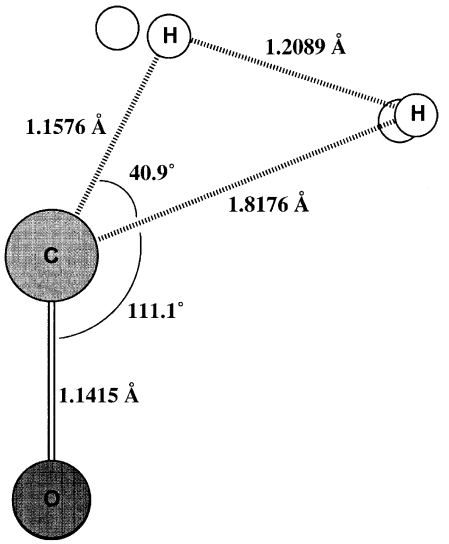

Fig. 6. The structure where the total occupation numbers of the CH bonds and HH bond valence bond structures are equal. The hydrogen atoms not bonded to the carbon atom represent the position at the transition state.

$$\varphi_{C1}\varphi_{C2}(\alpha\beta-\beta\alpha)\cdot\varphi_{H2}\varphi_{H2}\alpha\beta, \quad \text{(XIV)}$$

$$\varphi_{C1}\varphi_{C1}\alpha\beta\cdot\varphi_{H1}\varphi_{H1}\alpha\beta, \quad \text{(XV)}$$

$$\varphi_{H1}\varphi_{H1}\alpha\beta\cdot\varphi_{C2}\varphi_{C2}\alpha\beta, \quad \text{(XVI)}$$

$$\varphi_{C1}\varphi_{C1}\alpha\beta\cdot\varphi_{H2}\varphi_{H2}\alpha\beta, \quad \text{(XVII)}$$

$$\varphi_{H2}\varphi_{H2}\alpha\beta\cdot\varphi_{C2}\varphi_{C2}\alpha\beta, \quad \text{(XVIII)}$$

$$\varphi_{C1}\varphi_{C1}\alpha\beta\cdot\varphi_{C2}\varphi_{C2}\alpha\beta, \quad \text{(XIX)}$$

$$\varphi_{H1}\varphi_{H1}\alpha\beta\cdot\varphi_{H2}\varphi_{H2}\alpha\beta, \quad \text{(XX)}$$

where φ_{C1}, φ_{C2}, φ_{H1}, and φ_{H2} are non-orthogonal localized orbitals illustrated in Figs. 2 and 3.

Structures (I)–(IX) are classified as CH bond structures, and structures (X)–(XIV) as HH bond structures. Structures (XV)–(XX) are classified as neither of the above, since these structures can be regarded both as structures polarized further from one of (II)–(IX) and (XI)–(XIV).

Fig. 4 shows the changes in the occupation numbers of the covalent CH bonds, ionic CH bonds, covalent HH bond, ionic HH bond, and doubly ionic structures along the intrinsic reaction coordinate (IRC) in the non-orthogonal CASVB case. (Only the results of the non-orthogonal CASVB calculations are presented hereafter.) These are defined by:

$$n_{\text{Covalent CH}} = n_{\text{I}}, n_{\text{Ionic CH}} = \sum_{S=\text{II}}^{\text{IX}} n_S, \quad (45)$$

$$n_{\text{Covalent HH}} = \sum_{S=\text{X}}^{\text{XII}} n_S, n_{\text{Ionic HH}} = n_{\text{XIII}} + n_{\text{XIV}}, \quad (46)$$

and:

$$n_{\text{Doubly Pol.}} = \sum_{S=\text{XV}}^{\text{XX}} n_S. \quad (47)$$

The origin of the horizontal axis corresponds to the transition state structure, and the left end of each curve to the equilibrium structure. The occupation numbers of CH and HH covalent bond structures change rapidly near the transition state and the curves cross immediately after the transition state (0.1 bohr(amu)$^{1/2}$), while the occupation numbers of the CH and HH ionic bond structures change slowly.

Fig. 5 shows the changes in the total occupation numbers of the CH and HH bond structures along the IRC:

$$n_{\text{CH}} = n_{\text{Covalent CH}} + n_{\text{Ionic CH}}, n_{\text{HH}} = n_{\text{Covalent HH}} + n_{\text{Ionic HH}}. \quad (48)$$

The crossing point is located at the same point after the TS, 0.42 bohr(amu)$^{1/2}$ in both graphs. The structure corresponding to this point is shown in Fig. 6. Compared with the TS, the longer and shorter CH bonds have stretched by 0.14 and 0.06 Å, respectively, and the HH bond has shrunk by 0.18 Å. These bond lengths are 1.03, 1.62, and 1.80 times the equilibrium CH length, the other CH bonds of H_2CO, and the HH bond of H_2, respectively. That point is the structure where the bonds switch; in other words, the point is the *transition state* between the CH bonds and HH bond.

The observation described in this subsection implies that the total occupation number defined in Eqs. (48) is useful for providing a quantitative description of chemical bonds at transition states and along reaction paths.

3. Relativistic effect

It is well known that the relativistic effect is important in the study of systems including heavy atoms [38]. The Dirac equation is solved instead of the non-relativistic Schrödinger equation in order to treat the relativistic effect theoretically. The Dirac equation with the four-component spinors composed of the large (upper) and small (lower) components demands severe computational efforts to solve, and its applications to molecules are limited to small- to medium-size systems. Thus, several quasi-relativistic approximations have been proposed instead of explicitly solving the four-component relativistic Dirac equation.

The Breit–Pauli (BP) approximation [39] is obtained truncating the Taylor expansion of the Foldy–Wouthuysen transformed Dirac Hamiltonian [40] up to the $(p/mc)^2$ term. The BP equation has the well-known mass–velocity, Darwin, and spin–orbit operators. Although the BP equation gives reasonable results in the first-order perturbation calculation, it cannot be used in the variational treatment.

One of the shortcomings of the BP approach is that the expansion in $(p/mc)^2$ is not justified in the case where the electronic momentum is too large, e.g. for a Coulomb-like potential. The zeroth-order regular approximation (ZORA) [41,42] can avoid this disadvantage by expanding in $E/(2mc^2 - V)$ up to the first order. The ZORA Hamiltonian is variationally stable. However, the Hamiltonian obtained by a higher-order expansion has to be treated perturbatively, similarly to the BP Hamiltonian.

Recently, we have developed two quasi-relativistic approaches; one is the RESC method [43,44] and another is the higher-order Douglas–Kroll method [45,46]. In this section, we will review these theories and show their applications to the heavy-element systems.

3.1. RESC method

The Dirac equation has the four-component spinors,

$$\Psi = \begin{pmatrix} \Psi^{\mathrm{L}} \\ \Psi^{\mathrm{S}} \end{pmatrix}, \tag{49}$$

where Ψ^{L} and Ψ^{S} are the large (upper) and small (lower) components, respectively. Dirac spinor Ψ is normalized as

$$\langle \Psi | \Psi \rangle = \langle \Psi^{\mathrm{L}} | \Psi^{\mathrm{L}} \rangle + \langle \Psi^{\mathrm{S}} | \Psi^{\mathrm{S}} \rangle = 1, \tag{50}$$

while neither Ψ^{L} nor Ψ^{S} is normalized. The Dirac equation can be written as coupled equations,

$$V\Psi^{\mathrm{L}} + c(\boldsymbol{\sigma}\cdot\mathbf{p})\ \Psi^{\mathrm{S}} = E\ \Psi^{\mathrm{L}}, \tag{51a}$$

$$c(\boldsymbol{\sigma}\cdot\mathbf{p})\Psi^{\mathrm{L}} + (V - E - 2mc^2)\Psi^{\mathrm{S}} = 0, \tag{51b}$$

where $\boldsymbol{\sigma}$ stands for the 2×2 Pauli spin matrix vector. From Eq. (51b), the small component is expressed as

$$\Psi^{\mathrm{S}} = [2mc^2 - (V - E)]^{-1} c(\boldsymbol{\sigma}\cdot\mathbf{p})\ \Psi^{\mathrm{L}} \equiv X\Psi^{\mathrm{L}}. \tag{52}$$

By substitution of this equation into Eq. (51a), the Schrödinger–Pauli type equation composed of only the large component is obtained as

$$\left[V + (\boldsymbol{\sigma}\cdot\mathbf{p}) \frac{c^2}{2mc^2 - (V - E)} (\boldsymbol{\sigma}\cdot\mathbf{p}) \right] \Psi^{\mathrm{L}} = E\Psi^{\mathrm{L}}, \tag{53a}$$

and the normalization condition, Eq. (50), becomes

$$\langle \Psi^{\mathrm{L}} | 1 + X^{+}X | \Psi^{\mathrm{L}} \rangle = 1. \tag{53b}$$

Note that no approximation has been made so far. If we can solve Eq. (53a) with Eq. (53b), the Dirac solution can be obtained exactly.

However, it is difficult to solve this equation since Eq. (53a) has the energy and the potential in the denominator. An appropriate approximation has to be introduced. In our strategy, $E - V$ in the denominator is replaced by *the classical relativistic kinetic energy* (relativistic substitutive correction),

$$T = (m^2c^4 + p^2c^2)^{1/2} - mc^2. \tag{54}$$

The idea is simple and straightforward. This approach is referred to as the relativistic scheme by eliminating small components (RESC) [43,44]. The derivation of this approach is given in Ref. [43]. The resulting RESC Hamiltonian H_{RESC} can be separated into the spin-free (sf) and spin-dependent (sd) parts as

$$H_{\mathrm{RESC}} = H^{\mathrm{sf}}_{\mathrm{RESC}} + H^{\mathrm{sd}}_{\mathrm{RESC}}, \tag{55}$$

where

$$H^{\mathrm{sf}}_{\mathrm{RESC}} = T$$

Table 6
Equilibrium internuclear distances (r_e), vibrational frequencies (ω_e), dissociation energies (D_e), and the dipole moments (μ) of AgH in the ground state

Method	r_e (Å)	ω_e (cm^{-1})	D_e (eV)	μ (D)
Non-relativistic				
SCF	1.782	1521	1.09	–
MP2	1.705	1620	1.95	–
QCISD(T)	1.716	1504	2.15	–
MRMP	1.701	1617	1.99	–
BOP	1.710	1576	2.19	3.021
BLYP	1.704	1589	2.18	2.915
B3LYP	1.709	1598	2.24	3.322
Relativistic				
SCF	1.704	1635	1.19	–
MP2	1.622	1768	2.15	–
QCISD(T)	1.628	1720	2.35	–
MRMP	1.615	1794	2.19	–
BOP	1.632	1746	2.41	2.463
BLYP	1.628	1757	2.40	2.373
B3LYP	1.631	1761	2.44	2.760
Exptl.	1.618	1760	2.39	–

$$+OQ\mathbf{p}\cdot V\mathbf{p}QO^{-1} + 2mcOQ^{1/2}VQ^{1/2}O^{-1}, \tag{56}$$

and

$$H^{\mathrm{sd}}_{\mathrm{RESC}} = iOQ\boldsymbol{\sigma}\cdot(\mathbf{p}V)\times\mathbf{p}QO^{-1}. \tag{57}$$

Table 7
Equilibrium internuclear distances (r_e), vibrational frequencies (ω_e), dissociation energies (D_e), and the dipole moments (μ) of AuH in the ground state

Method	r_e (Å)	ω_e (cm^{-1})	D_e (eV)	μ (D)
Non-relativistic				
SCF	1.800	1602	1.14	–
MP2	1.679	1823	2.11	–
QCISD(T)	1.704	1683	2.26	–
MRMP	1.682	1847	2.75	–
BOP	1.724	1663	2.23	2.524
BLYP	1.719	1674	2.21	2.453
B3LYP	1.723	1689	2.27	2.821
Relativistic				
SCF	1.569	2145	1.95	–
MP2	1.479	2509	3.48	–
QCISD(T)	1.494	2440	3.57	–
MRMP	1.517	2337	3.32	–
BOP	1.533	2294	3.42	1.004
BLYP	1.531	2312	3.40	0.964
B3LYP	1.527	2328	3.40	1.238
Exptl.	1.524	2305	3.36	–

Here, O and Q operators are defined by

$$O = \frac{1}{E_p + mc^2}\left(1 + \frac{p^2c^2}{(E_p + mc^2)^2}\right)^{1/2}, \tag{58}$$

and

$$Q = \frac{c}{E_p + mc^2}, \tag{59}$$

where

$$E_p = (p^2c^2 + c^4)^{1/2}. \tag{60}$$

Although we have so far treated one-electron equation, the resulting equation can easily be extended to the many-electron case. For a practical calculation, the Hamiltonian matrix elements are evaluated in the space spanned by the eigenfunctions of the square momentum p^2 following Buenker and Hess [47,48], as well as the Douglas–Kroll–Hess (DKH) approach [48–50]. H_{RESC} is symmetrized to be Hermitian for mathematical convenience, instead of the physical significance.

The RESC approach has several advantages. It is variationally stable. This method can easily be implemented in various non-relativistic ab initio programs, and the relativistic effect is considered on the same footing with the electron correlation effect.

The RESC method was applied to the calculation of the spectroscopic constants of the ground state of AgH and AuH, which gives a good benchmark test, since the relativistic effect is very important for these molecules [43,44,51,52]. The electron correlation effect at various levels were treated: MP2 and QCISD(T) methods were used as the single-reference (SR) ab initio theory. The MRMP method [1–5] was employed as the multi-reference (MR)-based theory. For DFT, we employed the following exchange-correlation functionals; B88 [53] +OP [54] (BOP), B88 + LYP [55] (BLYP), and hybrid B3LYP [56].

The calculated equilibrium internuclear distances (r_e), harmonic vibrational frequencies (ω_e), dissociation energies (D_e), and the dipole moments (μ) of AgH and AuH are presented in Tables 6 and 7, respectively, together with the experimental data [25]. The non-relativistic results are poor even if electron correlation is included. Relativistic effect provides an obvious improvement of the results. The RESC

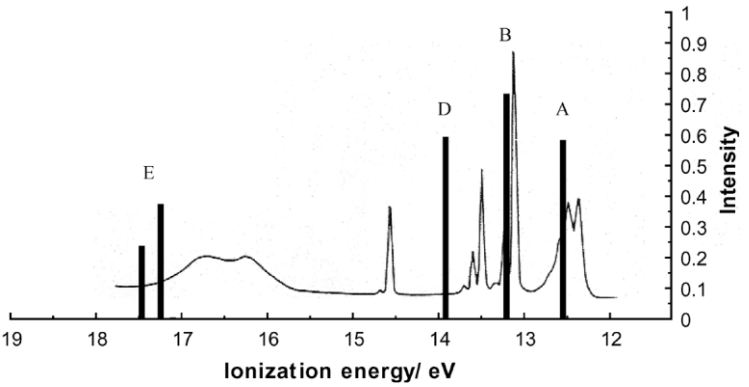

Fig. 7. The theoretical ionization spectrum of OsO_4 calculated by non-relativistic CASPT2.

approach gives a good agreement with experimental findings.

The calculated results of AgH are given in Table 6. The non-relativistic SCF computes r_e to be 1.782 Å, which is 0.16 Å longer than the experimental value, 1.618 Å. MP2, QCISD(T), and DFT reduce r_e by 0.06 Å, but it is still longer than the experimental value. The ω_e is computed to be smaller and the potential near the equilibrium geometry is too shallow. This situation is not improved even by a shift from the SR-based theory to the MR theory without the relativistic effect. The relativistic effect represents a great improvement over the non-relativistic theory. The r_e decreases by 0.08–0.09 Å from that of the non-relativistic theory, and the potential becomes much deeper. The D_e is also improved.

The AuH results are summarized in Table 7. The general trend for AuH is similar to that for AgH, but the relativistic effect is much more significant than the case of AgH. Non-relativistic SCF r_e is 0.276 Å longer than the experimental value, and the correlation effects remedy this by shortening r_e by 0.12 Å. However, r_e is still overestimated in the non-relativistic theory. The ω_e is again much smaller than the experimental value. The relativistic correction reduces r_e by 0.17–0.30 Å. Surprisingly, the relativistic effect increases ω_e by 490–760 cm^{-1}. The relativistic MRMP and DFT agree particularly well with the experimental value. Although the relativistic correction overwhelms the correlation effect in the r_e and ω_e for AuH, both effects are comparable as to D_e. In the case of AuH, as well as AgH, the relativistic effect is parallel to the electron correlation effect; both effects reduce r_e and increase ω_e and D_e.

The tetrahedral osmium oxide OsO_4 has been extensively studied by the photoelectron spectroscopy

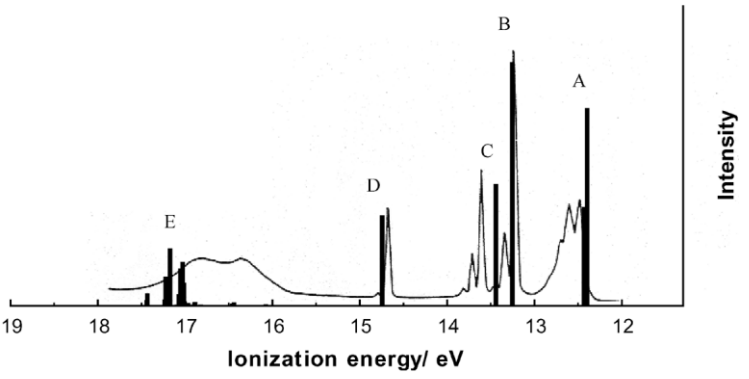

Fig. 8. The theoretical ionization spectrum of OsO_4 calculated by spin-orbit RESC-CASPT2.

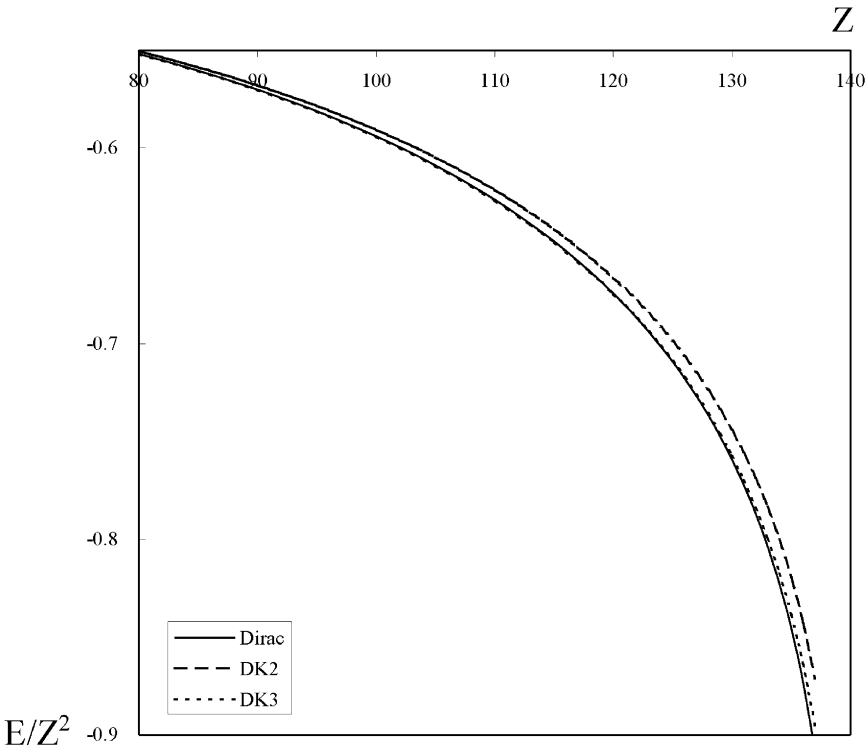

Fig. 9. E/Z^2 versus Z (nuclear charge) for 1s eigenvalues of hydrogen-like atoms.

(PES). The spectrum consists of five distinct band systems, called peaks A, B, C, D, and E. Unfortunately, the band assignments proposed differ in each of these PES studies. Furthermore, numerous ab initio computational and DFT approaches have been applied to this molecule with the aim of assigning the upper five valence ionization bands. However, some uncertainties still remain for assigning these bands mainly due to the occurrence of significant relativistic and correlation effects. There is no theoretical work studied by the method fully including both relativistic and correlation effects.

In this study, we clarify the whole range of the observed PES of OsO_4 by all-electron RESC-CASPT2 theory [57]. For the spin–orbit splitting, we used RESC-modified one-electron spin–orbit integrals, in which the charge of Os was scaled in order to compensate for the lack of two-electron spin–orbit integrals. The spin–orbit Hamiltonian, H_{SO}, derived from Eq. (57) was treated perturbatively. The spin–orbit eigenstates were obtained by diagonalizing $H_0 + H_{SO}$ in a basis of eigenfunctions of the unperturbed spin-free Hamiltonian H_0. In the present calculations, the diagonal elements of $H_0 + H_{SO}$ were substituted with CASPT2 energies, while the off-diagonal elements were calculated by CASSCF wave functions.

Figs. 7 and 8 show the non-relativistic and relativistic CASPT2 results, respectively. RESC-CASPT2 gives values for the peak positions and intensities in reasonable agreement with the resolved photoelectron spectrum data [58]. The Os valence 6s and 5p orbitals are expected to be stabilized while Os 5d orbitals are destabilized due to the relativistic effect. This change can be attributed to the change of the orbital (radial) part of the wave function, as is known well. The A band originating from O 2p MOs remains almost unchanged with the relativity. We can see that the peak C cannot be obtained without the relativity. This study confirms that the peak C arises from the spin–orbit coupling in the ionic $^2T_2(3t_2)$ states originated from the Os 5p orbitals. The observed intensity ratio of the B and C peaks is approximately 2: 1. This is fully supported by the present calculations. Peak

positions and intensities suggest that there is no doubt that this splitting could be associated with the bands B and C observed in PES. The peak D moves by 0.8 eV to the high energy side by the spin-free relativistic effects due to the stabilization of Os 6s orbital. The band D is originated from Os 6s and the peak position and intensity are rather insensitive to the spin–orbit effects. As shown in Ref. [57], the nondynamical relaxation effect is overestimated in the non-relativistic treatment, giving the weaker intensity, particularly to the satellite bands. This defect is improved by the spin-free relativistic RESC treatment. Under the E band, there are many two-electron shake-up peaks commencing at ca. 16.0 eV in addition to the two one-electron ionization peaks. The broad feature of the E band is due to these satellite peaks.

The RESC approach has been applied to various other systems in ground and excited states [52,59–63]. Since the energy gradient of the RESC method [64] is also available currently, we can study the chemical reaction in the heavy element systems.

3.2. Higher-order Douglas–Kroll method

The Douglas–Kroll (DK) transformation [49] can decouple the large and small components of the Dirac spinors in the presence of an external potential by repeating several unitary transformations. The DK transformation is a variant of the Foldy–Wouthuysen (FW) transformation [40], with an alternative natural expansion parameter, the external potential V_{ext} (or the coupling strength Ze^2), and avoids the high singularity in the FW transformation.

The first step in the DK transformation consists of a free-particle FW transformation in momentum space. Using the free-particle eigensolutions of the Dirac Hamiltonian associated with the positive energy eigenvalues, the unitary operator in the free-particle FW transformation is given as

$$U_0 = A(1 + \beta R), \tag{61}$$

where A and R are operators defined by

$$A = \left(\frac{E_p + c^2}{2E_p} \right)^{1/2}, \tag{62}$$

$$R = \frac{c\boldsymbol{\alpha}\cdot\mathbf{p}}{E_p + c^2}. \tag{63}$$

Application of this unitary operator to the Dirac Hamiltonian in the external field, $H_{\text{D}}^{\text{ext}}$, gives

$$H_1 = U_0 H_{\text{D}}^{\text{ext}} U_0^{-1} = \beta E_p + E_1 + O_1, \tag{64}$$

where E_1 and O_1 are the even and odd operators of first order in the external potential, respectively,

$$E_1 = A(V_{\text{ext}} + RV_{\text{ext}}R)A, \tag{65}$$

$$O_1 = \beta A(RV_{\text{ext}} - V_{\text{ext}}R)A. \tag{66}$$

Douglas and Kroll suggested that it is possible to remove odd terms of arbitrary orders in the external potential through successive unitary transformations

$$U_n = (1 + W_n^2)^{1/2} + W_n, \tag{67}$$

where W_n is an anti-Hermitian operator of order V_{ext}^n. The DK transformation correct to second order in the external potential has been extensively studied by Hess and co-workers [48,50], and has become one of the most familiar quasi-relativistic approaches. A numerical analysis by Molzberger and Schwarz [65] shows that the second-order DK (DK2) method recovers the energy up to the order of $Z^6\alpha^4$ to a large extent and includes also a significant part of the higher-order terms. However, the DK2 approach does not completely recover the stabilizing higher-order energy contributions, as shown in Fig. 9. The straightforward way to include higher-order relativistic effects is to repeat further unitary transformations. However, as far as we know, no higher-order DK Hamiltonians have explicitly appeared in the literature.

One reason for no appearance of higher-order DK Hamiltonians is that the derivation of the DK Hamiltonians of higher order in V_{ext} is too complicated, and it has been believed that the higher-order DK transformation appears to be impractical. Although Douglas and Kroll adopted Eq. (67) as a unitary operator in their formulation, the essence of the DK transformation is to remove odd terms by repeating *arbitrary* unitary transformations. Thus, in this study we adopt an exponential-type unitary operator of the form

$$U_n = \exp(W_n), \tag{68}$$

where W_n is anti-Hermitian. Expanding Eqs. (67) and (68) in a power series of W_n, we note that both expansions are common up to second order. One should

Table 8
SCF total and orbital energies (in au) for element 118 ($^1S_0$)

	NR	DK2	DK3	DFC[a]
Total energy	−46,324.2882	−54,347.2659	−54,587.2760	−55,026.3317
1s	−6222.6933	−8181.9300	−8279.9061	−8286.7260
2s	−1144.7046	−1728.6771	−1743.6418	−1742.6659
3s	−318.4622	−474.3213	−477.7972	−477.1589
4s	−95.3213	−142.0118	−143.0143	−142.7422
5s	−26.4226	−40.2208	−40.5232	−40.4269
6s	−5.7351	−9.0736	−9.1567	−9.1380
7s	−0.7740	−1.2969	−1.3136	−1.3279
2p	−1115.3498	−1263.2698	−1262.9243	−1313.6815
3p	−303.3611	−350.1415	−350.0165	−361.1473
4p	−87.6954	−101.5415	−101.4972	−104.5299
5p	−22.9045	−26.5021	−26.4859	−27.3553
6p	−4.3685	−4.9007	−4.8952	−5.1310
7p	−0.3944	−0.3917	−0.3905	−0.4436
3d	−275.4582	−274.2818	−274.2008	−274.0512
4d	−73.4531	−72.8418	−72.8127	−72.7125
5d	−16.4535	−15.7639	−15.7536	−15.7070
6d	−2.0211	−1.6153	−1.6126	−1.6021
4f	−53.3681	−48.9865	−48.9629	−48.7899
5f	−7.8674	−6.3582	−6.3510	−6.2995

[a] Averaged over fine structure components.

note that an exponential-type unitary operator, instead of a conventional form, is used in order to derive the higher-order DK Hamiltonians easily, since the exponential-type operator can take full advantage of the Hausdorff expansion.

Generally, the anti-Hermitian W_n of order V_{ext}^n determines the DK Hamiltonian (or its energy) to order $2n+1$ (referred to as the $2n+1$ rule) [45]. This $2n+1$ rule also simplifies the formulations of the high-order DK Hamiltonians significantly.

The resulting DK Hamiltonians are given as

$$H_{\text{DK2}} = \beta E_p + E_1 - \tfrac{1}{2}[W_1,[W_1,\beta E_p]], \tag{69}$$

$$H_{\text{DK3}} = H_{\text{DK2}} + \tfrac{1}{2}[W_1,[W_1,E_1]], \tag{70}$$

$$H_{\text{DK4}} = H_{\text{DK3}} - \tfrac{1}{8}[W_1,[W_1,[W_1,[W_1,\beta E_p]]]] + [W_2,[W_1,E_1]], \tag{71}$$

$$H_{\text{DK5}} = H_{\text{DK4}} + \tfrac{1}{24}[W_1,[W_1,[W_1,[W_1,E_1]]]] - \tfrac{1}{3}[W_2,[W_1,[W_1,[W_1,\beta E_p]]]], \tag{72}$$

where

$$W_1(p,p') = \beta\frac{O_1(p,p')}{E_{p'}+E_p}, \tag{73}$$

$$W_2(p,p') = \beta\frac{[W_1,E_1]}{E_{p'}+E_p}. \tag{74}$$

Note that W_2 is not included in the expression of the DK3 Hamiltonian as well as the DK2 Hamiltonian. This can simplify the practical calculation since the evaluation of the terms including the higher order W_n becomes complicated.

Although the DK formulas for the one-electron system are represented so far, the resulting formulas can easily be extended to the many-electron systems with the no-pair theory [66]. With the help of the no-pair projection, the two-component DK Hamiltonians including the two-electron terms are given by

$$H_+^{\text{DK1}} = \sum_i E_i - mc^2 + \sum_i V_{\text{eff}}(i) + \frac{1}{2}\sum_{i\neq j} V_{\text{eff}}(i,j), \tag{75}$$

$$H_+^{\mathrm{DK2}} = H_+^{\mathrm{DK1}} - \frac{1}{2}\sum_i [W_1(i), [W_1(i), E_i]_+]_+, \quad (76)$$

$$H_+^{\mathrm{DK3}} = H_+^{\mathrm{DK2}} + \frac{1}{2}\sum_i [W_1(i), [W_1(i), V_{\mathrm{eff}}(i)]], \quad (77)$$

with

$$E_i = (p_i^2c^2 + m^2c^4)^{1/2}, \quad (78)$$

$$V_{\mathrm{eff}}(i) = A_i[V_{\mathrm{ext}}(i) + (\boldsymbol{\sigma}_i\mathbf{R}_i)V_{\mathrm{ext}}(i)(\boldsymbol{\sigma}_i\mathbf{R}_i)]A_i, \quad (79)$$

$$V_{\mathrm{eff}}(i,j) = A_iA_j\Bigg[\frac{1}{r_{ij}} + (\boldsymbol{\sigma}_i\mathbf{R}_i)\frac{1}{r_{ij}}(\boldsymbol{\sigma}_i\mathbf{R}_i) + (\boldsymbol{\sigma}_j\mathbf{R}_j)\frac{1}{r_{ij}}(\boldsymbol{\sigma}_j\mathbf{R}_j) + (\boldsymbol{\sigma}_i\mathbf{R}_i) \times (\boldsymbol{\sigma}_j\mathbf{R}_j)\frac{1}{r_{ij}}(\boldsymbol{\sigma}_i\mathbf{R}_i)(\boldsymbol{\sigma}_j\mathbf{R}_j)\Bigg]A_iA_j, \quad (80)$$

$$A_i = \left(\frac{E_i + mc^2}{2E_i}\right)^{1/2}, \quad (81)$$

$$\mathbf{R}_i = \frac{c\mathbf{p}_i}{E_i + mc^2}, \quad (82)$$

where m is the mass, c the speed of light, $\mathbf{p}_i$ the momentum operator, and $\boldsymbol{\sigma}_i$ denotes the vector of three Pauli 2×2 spin matrices. Here, $W_1(i)$ is an integral operator with kernel

$$W_1(\mathbf{p}_i, \mathbf{p'}_i) = A_i(\mathbf{R}_i - \mathbf{R'}_i)A'_i\frac{V_{\mathrm{ext}}(\mathbf{p}_i, \mathbf{p'}_i)}{E_i - E'_i}, \quad (83)$$

and $[a,b]_+$ and $[a,b]$ denote the anti-commutator and the commutator, respectively. In Eq. (80), we omit the two-electron terms derived from the Breit operator, which are given explicitly in Ref. [66].

The DK approach has several advantages. It is variationally stable and can avoid the Coulomb singularity. The DK method can easily be incorporated into any kind of ab initio and DFT theory, as well as the RESC method [43,44]. Thus, one can handle the relativistic effect on the same footing with the electron correlation effect. We stress that modification of the one-electron integrals for the third-order relativistic correction with the DK3 Hamiltonian is not expensive in comparison with the DK2 Hamiltonian.

In order to illustrate the numerical performance of the DK3 approach, the result for one-electron systems is first presented [45]. The 1s eigenvalues of hydrogen-like atoms calculated by DK2 and DK3 methods are shown in Fig. 9 compared with the Dirac one in the same primitive Gaussian basis sets. The DK2 approach does not completely recover the stabilizing higher-order energy contributions. The DK3 method yields the excellent result. The third-order DK result improves on the second-order DK approximation and shows the DK3 Hamiltonian works well.

In Table 8, the SCF orbital energies of the $^1S_0$ ground state of element 118 ($7s^27p^6$) calculated with the DK3 Hamiltonian are shown in comparison with the DK2 Hamiltonian [45]. The SCF total energies of element 118 are also listed in Table 8. The non-relativistic (NR) Hartree–Fock (HF) and relativistic Dirac–Fock–Coulomb (DFC) results using the common primitive Gaussian set are also listed for comparison. In this calculation, the spin-dependent part in the DK Hamiltonian is neglected, resulting in a scalar relativistic variant of the method. The relativistic kinematics correction to the two-electron integrals is also ignored. This effect on the valence properties of molecules including the third-row transition metal has been shown to be small [67].

For the s orbital energies, where spin–orbit effect is not contributed, the DK3 result is in better agreement with the DFC result than the DK2 result. The total energy of element 118 is stabilized largely by 240 hartree with the third-order relativistic correction. This deviation is attributed mainly to the inner core s orbitals. It is also shown that the most significant improvement with the third-order scalar relativistic correction is achieved for the s orbitals. The third-order DK term in Eq. (77) is the correction to $V_{\mathrm{eff}}(i)$, which includes the operator, $\mathbf{p}\cdot V_{\mathrm{ext}}\mathbf{p}$, as shown in Ref. [45]. The $\mathbf{p}\cdot V_{\mathrm{ext}}\mathbf{p}$ operator may be reduced to the operator including the delta function when V_{ext} is a Coulomb potential. Thus, the third-order DK term affects the s orbitals, since the s orbitals have no node at the nucleus. The present results suggest that the third-order DK method is superior to the second-order DK method for the core-shell properties. The deviation between the DK3 and DFC total energies is about 440 hartree. This difference

Table 9
Spectroscopic constants of (112)H and its ions. (NR: non-relativistic, R: relativistic, *r*e: equilibrium internuclear distances in Å, ω_e: vibrational frequencies in cm^{-1}, B_e: rotational constants in cm^{-1}, D_e: dissociation energies in eV)

	$(112)H^+$			(112)H				$(112)H^-$		
Method	r_e	ω_e	B_e	r_e	ω_e	B_e	D_e	r_e	ω_e	B_e
HF										
NR-PP[a]	1.945	1663	–	–	–	–	–	–	–	–
NR	1.951	1653	4.408	2.031	1435	4.069	0.740	2.212	999	3.432
R-PP[a]	1.522	2687	–	–	–	–	–	–	–	–
DK2	1.525	2667	7.221	–[b]	–[b]	–[b]	–[b]	–[b]	–[b]	–[b]
DK3	1.526	2677	7.208	–[b]	–[b]	–[b]	–[b]	–[b]	–[b]	–[b]
MP2										
NR-PP[a]	1.883	1676	–	–	–	–	–	–	–	–
NR	1.894	1680	4.679	1.967	1495	4.337	0.438	2.174	974	3.552
R-PP[a]	1.507	2686	–	–	–	–	–	–	–	–
DK2	1.521	2617	7.254	1.816	1542	5.092	0.010	2.106	696	3.784
DK3	1.524	2615	7.225	1.812	1564	5.111	0.002	2.111	693	3.766
CCSD										
NR	1.936	1560	4.480	2.018	1346	4.121	0.860	2.203	954	3.458
DK2	1.525	2616	7.218	1.816	986	5.088	0.049	2.259	546	3.288
DK3	1.528	2621	7.186	1.823	991	5.052	0.036	2.273	533	3.250
CCSD(T)										
NR-PP[a]	1.929	1509	–	–	–	–	–	–	–	–
NR	1.941	1513	4.453	2.021	1318	4.109	0.804	2.204	945	3.457
R-PP[a]	1.515	2640	–	–	–	–	–	–	–	–
DK2	1.528	2584	7.186	1.824	999	5.043	0.068	2.224	591	3.394
DK3	1.532	2595	7.151	1.829	1007	5.017	0.057	2.234	582	3.364

[a] Pseudopotential calculation in Ref. [68].
[b] This state is totally repulsive.

is due to the energy stabilization by the spin–orbit effect for the p orbitals, as in the case of element 112[46].

Table 9 shows the spectroscopic constants of (112)H and its ions calculated with the DK2 and DK3 Hamiltonians compared to the non-relativistic results [46]. Among these molecules, only $(112)H^+$ has been studied so far using the pseudopotential (PP) approach [68], as also listed in Table 9.

On the whole, the third-order (scalar) relativistic corrections with the DK3 Hamiltonian are small compared with the second-order ones. The bonds are stretched by about 0.01 Å, and the rotational constants are decreased by 0.01–0.03 cm^{-1}. The harmonic vibrational frequencies are changed by a few wavenumbers. The dissociation energies of (112)H are decreased by about 0.01 eV.

Relativistic effects are significant for $(112)H^+$ and (112)H. The relativity decreases the bond lengths of $(112)H^+$ by 0.4 Å and those of (112)H by 0.2 Å with electron correlation effects. The vibrational frequencies of $(112)H^+$ are increased by 900–1000 cm^{-1}, and those of (112)H decreased by 300–350 cm^{-1} at the CCSD and CCSD(T) levels. The scalar relativistic effect on the properties of $(112)H^-$ is much smaller than those of $(112)H^+$ and (112)H. This is analogous to the behavior of isoelectronic (113)H studied previously by Seth et al. [69].

Electron correlation effects are important for (112)H and $(112)H^-$. While their potential energy curves are totally repulsive at the HF level, they have a minimum by a van der Waals or a dispersion interaction when electron correlation effects are included. For (112)H, the MP2 method seems to be inadequate and gives a large deviation in ω_e by inclusion of relativistic effects, compared to CCSD and CCSD(T).

The present findings suggest that the effect of the third-order (scalar) relativistic correction with the DK3 Hamiltonian is relatively small at least in

the valence-shell properties of the ground states of element 112, (112)H, and its ions. On the other hand, the improvement with the third-order relativistic correction is significant for the inner core shells, as shown by the atomic 118 and 112 results. Thus, a further investigation is needed on the influence of the third-order relativistic correction on other atomic and molecular systems in ground and excited states and other properties (especially, core-shell properties such as the NMR magnetic shielding constant) of systems including superheavy elements.

4. Density functional theory

Density functional theory (DFT) is a widely-used methodology in computational chemistry that solves a nonlinear equation—the Kohn–Sham equation—with an average-field potential of density functional. Because this methodology can incorporate electron correlation as a potential, it requires much less computational power to give equivalent chemical properties of molecules compared to high-level ab initio molecular orbital theories. The Kohn–Sham equation is given by [70,71]

$$\left[-\frac{1}{2}\nabla^2 + v + \int \frac{\rho(\mathbf{R}')}{|\mathbf{R}-\mathbf{R}'|}\mathrm{d}^3\mathbf{R}' + \frac{\delta E_{xc}[\rho]}{\delta\rho} \right]\psi_i = \epsilon_i\psi_i, \tag{84}$$

$$E = \sum_i^N \int \psi_i^*(-\frac{1}{2}\nabla^2 + v)\psi_i \mathrm{d}^3\mathbf{R} + \frac{1}{2}\int \frac{\rho(\mathbf{R})\rho(\mathbf{R}')}{|\mathbf{R}-\mathbf{R}'|}\mathrm{d}^3\mathbf{R}\mathrm{d}^3\mathbf{R}' + E_{xc}[\rho], \tag{85}$$

where v is an external field, and ρ is the density calculated by the molecular orbital ψ_i: $\rho = \sum_i^{occ} |\psi_i|^2$. Atomic units are used ($h = e^2 = m = 1$, energies are in hartree and distances in bohr). In Eqs. (84) and (85), the exchange integral operator in the Hartree–Fock (HF) equation is substituted by an exchange-correlation density functional E_{xc} and the potential $\delta E_{\mathrm{xc}}/\delta\rho$. Hence, the reliability of DFT depends on the functional used.

The functional should be tested by examining whether they

1. satisfy the fundamental conditions of the exact functional,
2. are applicable to a wide class of problems and a wide variety of systems,
3. have a simple form with a minimum number of parameters (including fundamental constants),
4. contain no additional parts for obtaining specific properties, and
5. have a progressive form that can be updated.

Almost all conventional development of correlation functionals has concentrated on satisfying criteria (1) and (2), while criteria (3)–(5) have received much less attention. In consequence, many semi-empirical parameters have been introduced to give accurate energies and exact functional properties, several functionals have been adjoined in order to reproduce a few properties, and the form has lacked in flexibility for the development of DFT [72]. These may lead to the lack of physical meaning and a poor reliability of DFT.

Recently, we developed exchange and correlation functionals: the parameter-free (Pfree) exchange [73] and the one-parameter progressive correlation (OP) [74] functionals. They have been shown to satisfy significant and strict fundamental conditions and give practical atomic exchange and correlation energies. By combining these functionals, we obtain an exchange-correlation functional that has only one parameter and no additional parts for obtaining specific properties. Surprisingly, it was found that the fundamental conditions of the exact kinetic, exchange, and correlation functionals are transversely connected with each other through this exchange-correlation functional called the 'POP' functional [75].

In this section, we introduce the OP correlation and the Pfree exchange functionals, and then describe the transversing connection between the fundamental conditions of the exact kinetic, exchange, and correlation functionals. The numerical investigations of these functionals are also presented for the exchange and correlation energies of atoms [75], the chemical properties of the G2 set of molecules [54,74], and the atomization energies of the first- to third-row transition metal dimers [75,76].

4.1. The one-parameter progressive correlation functional

We developed a simple Colle–Salvetti (CS)-type

correlation functional called the one-parameter progressive (OP) correlation functional [54,77]. The functional contains only one parameter and is adapted to any kind of exchange functional through the correlation length.

First, the spin-polarized CS-type correlation wavefunction is defined for opposite-spin electron pairs ($\sigma_1 \neq \sigma_2$) as [78]

$$\Psi_{\sigma_1\sigma_2}(\mathbf{x}_1, \mathbf{x}_2, \ldots, \mathbf{x}_N) = \Psi^{HF}_{\sigma_1\sigma_2}(\mathbf{x}_1, \mathbf{x}_2, \ldots, \mathbf{x}_N) \prod_{i>j} [1 - \phi_{\sigma_1\sigma_2}(\mathbf{r}_1, \mathbf{r}_j)], \quad (86)$$

where $\mathbf{r}_i$ indicates the spatial part of the spatial–spin-coordinates $\mathbf{x}_i$ of the i-th electron, and σ_1 and σ_2 are opposite spin indices having possible values α or β. The function $\Psi^{\mathrm{HF}}_{\sigma_1\sigma_2}$ is defined as a spin-polarized HF wavefunction that is multiplied by itself to obtain a spin-polarized HF second-order reduced density matrix for spin $\sigma_1\sigma_2$ pairs, $P^{\sigma_1\sigma_2}_{2\mathrm{HF}}$. The function $\phi_{\sigma_1\sigma_2}$ satisfies the spin-polarized correlation cusp conditions [79,80] by

$$\phi_{\sigma_1\sigma_2}(\mathbf{r}_1, \mathbf{r}_2) = \exp(-\beta^2_{\sigma_1\sigma_2} r^2)[1 - (1 + \lambda r/2)\Phi_{\sigma_1\sigma_2}(\mathbf{R})], \quad (87)$$

where $r = |\mathbf{r}_i - \mathbf{r}_j|, R = (\mathbf{r}_i + \mathbf{r}_j)/2$ and λ is the coupling strength. Under the assumption that the HF first-order density matrix is a good approximation to the exact one, the function $\Phi_{\sigma_1\sigma_2}(\mathbf{R})$ can be described approximately by

$$\Phi_{\sigma_1\sigma_2} \cong \frac{\sqrt{\pi}\beta_{\sigma_1\sigma_2}}{\sqrt{\pi}\beta_{\sigma_1\sigma_2} + \lambda}. \quad (88)$$

In Eq. (86), no correlation contribution is given for adiabatically unconnected independent-electron systems, because $\Psi_{\sigma_1\sigma_2}$ is $\Psi^{\mathrm{HF}}_{\sigma_1\sigma_2}$ for $\lambda = 0$.

To obtain the parameter $\beta_{\sigma_1\sigma_2}$, we used Becke's definition of correlation length [81]. Becke suggested that the correlation length $Z_{\sigma_1\sigma_2}$ can be defined as

$$Z_{\sigma_1\sigma_2} = const.\left(\frac{1}{\langle r^{-1}_{\sigma_1}\rangle} + \frac{1}{\langle r^{-1}_{\sigma_2}\rangle}\right), \quad (89)$$

for the exchange energy in the form

$$E_{\mathrm{x}} = -\frac{1}{2}\sum_{\sigma}\int \rho_\sigma \langle r^{-1}_\sigma\rangle d^3\mathbf{R}, \quad (90)$$

where ρ_σ is the electron density of spin σ. $\langle r^{-1}_\sigma\rangle$ is the mean inverse radius of a Fermi hole. Now, we assume that the exchange energy is written as a usual generalized-gradient-approximation (GGA) form,

$$E_x = -\frac{1}{2}\sum_{\sigma}\int \rho^{4/3}_\sigma K_\sigma d^3\mathrm{R}, \quad (91)$$

where $x_\sigma = |\nabla\rho_\sigma|/\rho^{4/3}_\sigma$. We then obtain the correlation length $Z_{\sigma_1\sigma_2}$

$$Z_{\sigma_1\sigma_2} = const.(\rho^{-1/3}_{\sigma_1} K^{-1}_{\sigma_1} + \rho^{-1/3}_{\sigma_2} K^{-1}_{\sigma_2}). \quad (92)$$

Because the volume of the exchange potential $V_{\sigma_1\sigma_2}$ should be proportional to a sphere with radius half the correlation length, we obtain [77]

$$V_{\sigma_1\sigma_2} = const.\frac{4\pi}{3}\left(\frac{Z_{\sigma_1\sigma_2}}{2}\right)^3. \quad (93)$$

Following Colle and Salvetti, we assume that $V_{\sigma_1\sigma_2}$ is proportional to the volume of the region where the correlation energy differs appreciably from zero,

$$\int \exp(-\beta^2_{\sigma_1\sigma_2} r^2) d^3\mathbf{r} = \frac{\pi^{3/2}}{\beta^3_{\sigma_1\sigma_2}}. \quad (94)$$

The spin-polarized exponent coefficient $\beta_{\sigma_1\sigma_2}$ is then given by

$$\beta_{\sigma_1\sigma_2} = q_{\sigma_1\sigma_2}\frac{\rho^{1/3}_{\sigma_1}\rho^{1/3}_{\sigma_2} K_{\sigma_1} K_{\sigma_2}}{\rho^{1/3}_{\sigma_1} K_{\sigma_1} + \rho^{1/3}_{\sigma_2} K_{\sigma_2}}, \quad (95)$$

where $q_{\sigma_1\sigma_2}$ is a parameter that determines the correlation length.

By using Eq. (86) and the correlated spin-polarized second-order density matrix $P^{\sigma_1\sigma_2}_2 = |\Psi_{\sigma_1\sigma_2}|^2$, the spin-polarized CS-type correlation functional is obtained for opposite-spin pairs,

$$E^{\sigma_1\sigma_2}_c = \int (P^{\sigma_1\sigma_2}_2(\mathbf{r}_1, \mathbf{r}_2) - P^{\sigma_1\sigma_2}_{2\mathrm{HF}}(\mathbf{r}_1, \mathbf{r}_2)) r^{-1} \mathrm{d}^3\mathbf{r}_1 \mathrm{d}^3\mathbf{r}_2 = \int P^{\sigma_1\sigma_2}_{2\mathrm{HF}}(\mathbf{r}_1, \mathbf{r}_2) r^{-1} (\phi^2_{\sigma_1\sigma_2}(\mathbf{r}_1, \mathbf{r}_2) - 2\phi_{\sigma_1\sigma_2}(\mathbf{r}_1, \mathbf{r}_2)) \mathrm{d}^3\mathbf{r}_1 \mathrm{d}^3\mathbf{r}_2. \quad (96)$$

Then, we used the angle-averaged Taylor expansion of $P^{\sigma_1\sigma_2}_{2\mathrm{HF}}$. Based on the assumption that electron correlation acts only between two opposite-spin electrons that come close to each other, the expansion was limited to the first-order in order to keep the balance

with GGA-type exchange functionals:

$$\int P_{2HF}^{\sigma_1\sigma_2}\left(\mathbf{R}+\frac{\mathbf{r}}{2},\mathbf{R}-\frac{\mathbf{r}}{2}\right)r^{-1}\exp(-\beta_{\sigma_1\sigma_2}^2 r^2)\mathrm{d}^3\mathbf{r}$$

$$\cong 4\pi P_{2\mathrm{HF}}^{\sigma_1\sigma_2}(\mathbf{R},\mathbf{R})\int_0^\infty r\exp(-\beta_{\sigma_1\sigma_2}^2 r^2)\mathrm{d}r, \qquad (97)$$

where $r=|\mathbf{r}|=|\mathbf{r}_i-\mathbf{r}_j|$ and $\mathbf{R}=(\mathbf{r}_i+\mathbf{r}_j)/2$ for each electron-pair, (i, j). The first-order term disappears due to the angle-averaged integration. We should notice that the angle-averaged Taylor expansion of the diagonal term of the HF second-order reduced density matrix for parallel-spin pairs $\int P_{2\mathrm{HF}}^{\sigma\sigma}$ up to the first-order is zero in the angle-averaged integration due to the Pauli exclusion principle:

$$\int P_{2HF}^{\sigma\sigma}\left(\mathbf{R}+\frac{\mathbf{r}}{2},\mathbf{R}-\frac{\mathbf{r}}{2}\right)r^{-1}\exp(-\beta_{\sigma\sigma}^2 r^2)\mathrm{d}^3\mathbf{r}\cong 0. \qquad (98)$$

Hence, the correlation energy for parallel-spin pairs can be neglected, because it is also described by using Eq. (96) as $\sigma_1=\sigma_2$. By using Eqs. (97) and (98), the correlation energy is written as

$$E_c^\lambda = E_c^{\alpha\beta}+E_c^{\beta\alpha}$$

$$= -4\pi\int\rho_\alpha\rho_\beta\left[2\int\exp(-\beta_{\alpha\beta}^2 r^2)\times(1-\Phi_{\alpha\beta}(1+\frac{\lambda r}{2}))r\mathrm{d}r-\int\exp(-2\beta_{\alpha\beta}^2 r^2)\times(1-\Phi_{\alpha\beta}(1+\frac{\lambda r}{2}))^2 r\mathrm{d}r\right]\mathrm{d}^3\mathbf{R}, \qquad (99)$$

In the derivation, we used $P_{2HF}^{\alpha\beta}(\mathbf{R},\mathbf{R})=\rho_\alpha(\mathbf{R})\rho_\beta(\mathbf{R})/2$. Substituting Eqs. (88) and (95) into Eq. (99) gives

$$E_c=-\int\rho_\alpha\rho_\beta\frac{1.5214\beta_{\alpha\beta}+0.5764}{\beta_{\alpha\beta}^4+1.1284\beta_{\alpha\beta}^\beta+0.3183\beta_{\alpha\beta}^2}d^3\mathbf{R}, \qquad (100)$$

where the coupling strength λ is replaced by 1 for simplicity. The only semi-empirical parameter $q_{\alpha\beta}$ is determined for each exchange functional.

4.2. The parameter-free exchange functional

We also developed a simple analytic exchange functional called the parameter-free (Pfree) exchange functional that contains no parameter [73]. The Pfree exchange functional is based on a density matrix expansion (DME) derived from a spin-polarized HF first-order density matrix by using spherical Bessel functions (j_n) up to the second-order [82]

$$P_{1\sigma}^{\mathrm{DME}}\left(\mathbf{R}+\frac{\mathbf{r}}{2},\mathbf{R}-\frac{\mathbf{r}}{2}\right)=\frac{3j_1(k_\sigma r)}{k_\sigma r}\rho_\sigma(\mathbf{R})+\frac{35j_3(k_\sigma r)}{2k_\sigma^3 r}\times\left(\frac{\nabla^2\rho_\sigma(\mathbf{R})}{4}-\tau_\sigma(\mathbf{R})+\frac{3}{5}k_\sigma^2\rho_\sigma(\mathbf{R})\right)+\cdots. \qquad (101)$$

The kinetic energy density, τ_σ, is defined in the form of the HF non-interacting kinetic energy,

$$T_s=\frac{1}{2}\sum_\sigma\int\sum_i^{occ}|\nabla\psi_{i\sigma}|^2\mathrm{d}^3\mathbf{R}=\frac{1}{2}\sum_\sigma\int\tau_\sigma\mathrm{d}^3\mathbf{R}. \qquad (102)$$

By using Eq. (101), the DME of the HF exchange energy becomes as [83]

$$E_x^{\mathrm{DME}}[\rho_\sigma,k_\sigma,\tau_\sigma]$$

$$=-\frac{1}{2}\sum_\sigma\int|P_{1\sigma}^{\mathrm{DME}}\left(\mathbf{R}+\frac{\mathbf{r}}{2},\mathbf{R}-\frac{\mathbf{r}}{2}\right)|^2 r^{-1}\mathrm{d}^3\mathbf{R}\mathrm{d}^3\mathbf{r}$$

$$\cong-\frac{\pi}{2}\sum_\sigma\int\left[\frac{9}{k_\sigma^2}\rho_\sigma^2+\frac{35}{3k_\sigma^4}\rho_\sigma\times\left(\frac{\nabla^2\rho_\sigma}{4}-\tau_\sigma+\frac{3}{5}k_\sigma^2\rho_\sigma\right)\right]\mathrm{d}^3\mathbf{R}. \qquad (103)$$

By a partial integration [84], the Laplacian term $\nabla^2\rho_\sigma$ can be eliminated from Eq. (103):

$$E_x^{\mathrm{DME}}[\rho_\sigma,k_\sigma,\tau_\sigma]$$

$$=-\frac{\pi}{2}\sum_\sigma\int\left[\frac{9}{k_\sigma^2}\rho_\sigma^2+\frac{35}{3k_\sigma^4}\rho_\sigma^{8/3}\left(\frac{x_\sigma^2}{12}-z_\sigma\right)\right]\mathrm{d}^3\mathbf{R}, \qquad (104)$$

where x_σ and z_σ are dimensionless parameters that can be expressed as $x_\sigma=|\nabla\rho_\sigma|/\rho_\sigma^{4/3}$ and $z_\sigma=(\tau_\sigma-3k_\sigma^2\rho_\sigma/5)/\rho_\sigma^{5/3}$.

The momentum, k_σ, has been substituted by the Fermi momentum, $k_{F\sigma}=(6\pi^2\rho_\sigma)^{1/3}$ or the correction [83–85]. By getting back to the original of DME [82], we regard k_σ as the averaged relative momentum at each center-of-mass coordinate $\mathbf{R}$, and express it as a

Table 10
Some strict physical conditions for K_σ in the exact exchange functional, $E_x - (1/2)\sum_\sigma \int \rho_\sigma^{4/3} K_\sigma d^3\mathbf{R}$, and for H in the exact correlation functional, $E_c = -\int \rho_\alpha \rho_\beta H d^3\mathbf{R}$. In conditions (B)–(D), λ is a coordinate-scaling parameter. In condition (G), ρ_1 is the density for a one-electron system

	Conditions	LSDA	PW91	PBE	B88	LYP	POP
(A)	$K_\sigma > 0$	Yes	Yes	Yes	Yes	–	Yes
	$H \geq 0$	Yes	No	Yes	–	No	Yes
(B)	$K_\sigma[\rho_\lambda] = const.$	Yes	Yes	Yes	Yes	–	Yes
	$H[\rho_\lambda] > \lambda H[\rho]$ $(\lambda < 1)$	Yes	Yes	Yes	–	No	Yes
	$\lim_{\lambda\to\infty}\lambda^3 H[\rho_\lambda] = const. \neq 0$	No	No	Yes	–	Yes	Yes
	$\lim_{\lambda\to 0}\lambda^2 H[\rho_\lambda] = const. \neq 0$	Yes	Yes	Yes	–	Yes	Yes
(C)	$\lim_{\lambda\to 0,\infty}\lambda^{1/3} K_\sigma[\rho_\lambda^x] = const. \neq 0$	No	No	No	No	–	–
	$\lim_{\lambda\to 0,\infty}\lambda^{1/3} H[\rho_\lambda^x] = const. \neq 0$	No	Yes	No	–	No	Yes
(D)	$\lim_{\lambda\to 0,\infty}\lambda^{-1/3} K_\sigma[\rho_{\lambda\lambda}^{xy}] = const. \neq 0$	No	No	No	No	–	–
	$\lim_{\lambda\to\infty}\lambda^3 H[\rho_{\lambda\lambda}^{xy}] = const. \neq 0$	No	Yes	No	–	No	Yes
	$\lim_{\lambda\to 0}\lambda^2 H[\rho_{\lambda\lambda}^{xy}] = const. \neq 0$	No	Yes	No	–	No	Yes
(E)	$K_\sigma = 3(3/4\pi)^{1/3}$ for $const.\rho$	Yes	Yes	Yes	Yes	–	Yes
	$\lim_{\rho\to\infty} H = 0$ for $const.\ \rho$	Yes	Yes	Yes	–	No	Yes
	$\lim_{\rho\to 0}\rho^{2/3} H = const. \neq 0$ for $const.\ \rho$	No	No	No	–	No	Yes
(F)	Exact GGA of K_σ for slowly varying ρ	–	Yes?	Yes?	No	–	Yes?
	Exact GGA of H for slowly varying ρ	–	Yes	Yes	–	No	Yes
(G)	$K_\sigma = O(q^{2/3})$ for $\rho_q = q\rho_1 (0 < q \leq 1)$	No	No	No	No	–	Yes
	$H = 0$ for $\rho_q = q\rho_1 (0 < q \leq 1)$	No	No	No	–	Yes	Yes
(H)	$\lim_{R\to\infty} K_\sigma = \rho_\sigma^{-1} R^{-1}$	No	No	No	Yes?	–	No
	$K_\sigma < 4.231$	Yes	Yes	Yes	No	–	–

functional of the kinetic energy density, $\tau_\sigma(\mathbf{R})$. There is a natural relation between τ_σ and k_σ:

$$\tau_\sigma(\mathbf{R}) = 2\left\langle \frac{\mathbf{k}^2}{2} \right\rangle \rho_\sigma(\mathbf{R}) = \frac{\int \mathbf{k}^2 f_\sigma(\mathbf{R},\mathbf{k}) d^3\mathbf{k}}{\int f_\sigma(\mathbf{R},\mathbf{k}) d^3\mathbf{k}} \rho_\sigma(\mathbf{R})$$

$$= \frac{3}{5} k_\sigma^2(\mathbf{R}) \rho_\sigma(\mathbf{R}). \quad (105)$$

In Eq. (105), the distribution function, $f_\sigma(\mathbf{R},\mathbf{k})$, for the spin-polarized first-order density matrix in Eq. (101), is approximated by using the step function, $\Theta(k_\sigma - |\mathrm{k}|)$, in the momentum space, such that

$$f_\sigma(\mathrm{R},\mathrm{k}) = \frac{1}{(2\pi)^3} \int P_{1\sigma}^{\mathrm{DME}}\left(\mathrm{R} + \frac{\mathrm{r}}{2}, \frac{\mathrm{r}}{2}\right) \exp(-i\mathrm{k}\cdot\mathrm{r}) d^3\mathrm{r}$$

$$\approx const.\rho_\sigma(\mathrm{R}) \Theta(k_\sigma - |\mathbf{k}|). \quad (106)$$

The averaged relative momentum is thought to be identical with the center-of-mass one that is calculated by the kinetic energy density at the position. From Eq. (105), k_σ is written inversely as

$$k_\sigma = \sqrt{\frac{5\tau_\sigma}{3\rho_\sigma}}. \quad (107)$$

Substituting Eq. (107) into Eq. (104) gives a simple τ_σ-dependent DME exchange functional,

$$E_x^P[\rho_\sigma, \nabla\rho_\sigma, \tau_\sigma]$$

$$= -\frac{1}{2}\sum_\sigma \int \frac{27\pi}{5\tau_\sigma} \rho_\sigma^3 \left[1 + \frac{7x_\sigma^2 \rho_\sigma^{5/3}}{108\tau_\sigma}\right] d^3\mathbf{R}. \quad (108)$$

This functional contains no adjusted parameter and no additional parts for obtaining specific properties. If τ_σ equals the Thomas–Fermi (TF) kinetic energy density, $\tau_\sigma^{\mathrm{TF}} = (3/5)(6\pi^2)^{2/3}\rho_\sigma^{5/3}$, k_σ becomes identical to $k_{F\sigma} = (6\pi^2\rho_\sigma)^{1/3}$ for the non-interacting

system, and therefore, E_x^{Pfree} in Eq. (108) perfectly reproduces the local spin density approximation (LSDA) for exchange energy for $\nabla\rho_\sigma = 0$. The higher-order terms are neglected in Eq. (108) [85], because it may be hard to obtain the stable values of $(x_\sigma^2/\tau_\sigma)^n$ for $n \geq 2$ in the numerical computation.

4.3. A transversing connection between kinetic, exchange, and correlation functionals

By using the Pfree exchange and OP correlation functionals, the fundamental conditions for exact kinetic, exchange, and correlation functionals are shown to be transversely connected from each other, despite they have been independently suggested[74]. For simplicity, we introduce three parameters, T_σ, K_σ^{P}, and H^{OP}. T_σ is defined using a GGA form of non-interacting kinetic energy:

$$T_s \equiv \frac{1}{2}\sum_\sigma \int \rho_\sigma^{5/3} T_\sigma \mathrm{d}^3\mathbf{R}. \tag{109}$$

Substituting T_σ into Eq. (108) gives K_σ in Eq. (91) for the Pfree exchange functional:

$$K_\sigma^{\mathrm{P}}[x_\sigma, T_\sigma] = \frac{27\pi}{5T_\sigma}\left[1 + \frac{7x_\sigma^2}{108T_\sigma}\right]. \tag{110}$$

For K_σ^{P}, the fractional part of the OP correlation functional in Eq. (100), H^{OP} is given by

$$H^{\mathrm{OP}}[\beta_{\alpha\beta}^{\mathrm{P}}] = \frac{1.5214\beta_{\alpha\beta}^{\mathrm{P}} + 0.5764}{\beta_{\alpha\beta}^{\mathrm{P4}} + 1.1284\beta_{\alpha\beta}^{\mathrm{P3}} + 0.3183\beta_{\alpha\beta}^{\mathrm{P2}}}, \tag{111}$$

where

$$\beta_{\alpha\beta}^{\mathrm{P}}[\rho_\sigma, \rho_\beta, K_\alpha^P, K_\beta^{\mathrm{P}}] = q_{\alpha\beta}\frac{\rho_\alpha^{1/3}\rho_\beta^{1/3}K_\alpha^{\mathrm{P}}K_\beta^{\mathrm{P}}}{\rho_\sigma^{1/3}K_\alpha^{\mathrm{P}} + \rho_\beta^{1/3}K_\beta^{\mathrm{P}}}, \tag{112}$$

We make clear the relationship between these parameters. Table 10 shows which of the fundamental conditions for K_σ and H are met by the POP functional and conventional famous functionals; LSDA [86,87], Perdew–Wang 1991 (PW91) exchange-correlation [88], Perdew–Burke–Ernzerhof (PBE) exchange-correlation [72], Becke 1988 (B88) exchange [53], and Lee–Yang–Parr (LYP) correlation [55] functionals.

(A) Kinetic energy is positive for any non-zero density, $T_\sigma > 0$. Hence, K_σ^{P} in Eq. (110) is definitely positive for any non-zero density, $K_\sigma^{\mathrm{P}} > 0$ [73,89]. H^{OP} is positive or zero (only if ρ_β is zero) for any density [54,89], $H^{\mathrm{OP}} \geq 0$ because $\beta_{\alpha\beta}$ is always positive for a positive K_σ.

(B) Under uniform scaling of all coordinates $(\rho(R_x, R_y, R_z) \rightarrow \rho_\lambda = \lambda^3\rho(\lambda R_x, \lambda R_y, \lambda R_z))$, T_σ is scaled as [90]

$$T_\sigma[\rho_\lambda] = const. \neq 0. \tag{113}$$

For a constant T_σ, it has been shown that K_σ^P is scaled as

$$K_\sigma^{\mathrm{P}}[\rho_\lambda] = const. \neq 0. \tag{114}$$

This is one of the fundamental conditions of the exact exchange functional [89]. For a constant K_σ^P, it has been shown that H^{OP} has the following scaling properties:

$$H^{\mathrm{OP}}[\rho_\lambda] > \lambda H^{\mathrm{OP}}[\rho](\lambda < 1), \tag{115}$$

$$H^{OP}[\rho_\lambda] < \lambda H^{\mathrm{OP}}[\rho](\lambda > 1), \tag{116}$$

and in the high- and low-density limits,

$$\lim_{\lambda\to 0}\lambda^3 H^{\mathrm{OP}}[\rho_\lambda] = const. \neq 0, \tag{117}$$

$$\lim_{\lambda\to 0}\lambda^2 H^{\mathrm{OP}}[\rho_\lambda] = const. \neq 0, \tag{118}$$

respectively. Eqs. (115)–(118) correspond to the fundamental conditions of the exact correlation functional [89].

(C) For non-uniform scaling of the x coordinate $(\rho(R_x, R_y, R_z) \rightarrow \rho_\lambda^x = \lambda\rho(\lambda R_x, \lambda R_y, \lambda R_z))$, there is no equality for the non-uniform scaling of T_σ [90]. Hence, we cannot determine the λ-dependency of K_σ^{P} from that of T_σ. The exact λ-dependency of K_σ itself is given as [91,92]

$$\lim_{\lambda\to 0,\infty}\lambda^{1/3}K_\sigma[\rho_\lambda^x] = const. \neq 0. \tag{119}$$

Note that the λ-dependency of T_σ cannot be determined from K_σ^{P}. These conditions may, therefore, be essential for electron–electron interactions. If

K_σ satisfies Eq. (119), H^{OP} reproduces the non-uniform scaling condition [93,94],

$$\lim_{\lambda\to 0,\infty} H^{\mathrm{OP}}[\rho_\lambda^x] = const. \neq 0. \tag{120}$$

(D) Under non-uniform scaling of x and y coordinates ($\rho(R_x, R_y, R_z) \to \rho_{\lambda\lambda}^{xy} = \lambda^2\rho(\lambda R_x, \lambda R_y, R_z)$), no relation also exists for this scaling of T_σ [90], and, therefore, the λ-dependency of K_σ^{P} cannot be determined from that of T_σ. The exact λ-dependency of K_σ itself is given as [91,92]

$$\lim_{\lambda\to 0,\infty} \lambda^{-1/3} K_\sigma[\rho_{\lambda\lambda}^{xy}] = const. \neq 0. \tag{121}$$

The λ-dependency of K_σ is also intrinsic for this scaling, because the λ-dependency of T_σ cannot be determined from K_σ^{P}. For the exact K_σ, H^{OP} satisfies [93,94]

$$\lim_{\lambda\to\infty} \lambda^3 H^{\mathrm{OP}}[\rho_{\lambda\lambda}^{xy}] = const. \neq 0, \tag{122}$$

$$\lim_{\lambda\to 0} \lambda^2 H^{\mathrm{OP}}[\rho_{\lambda\lambda}^{xy}] = const. \neq 0. \tag{123}$$

(E) For a constant density ($x_\sigma = 0$), T_σ has an LSDA limit that corresponds to that of the Thomas–Fermi kinetic energy [71]

$$T_\sigma = T_\sigma^{\mathrm{LSDA}} = \frac{3}{5}(6\pi^2)^{2/3}. \tag{124}$$

For T_σ^{LSDA} and $x_\sigma = 0$, K_σ^P reduces to the K_σ of the LSDA exchange functional, K_σ^{LSDA} [71,73],

$$K_\sigma^P = K_\sigma^{\mathrm{LSDA}} = 3\left(\frac{3}{4\pi}\right)^{1/3}. \tag{125}$$

As far as we know, all conventional GGA-type exchange functions give K_σ^{LSDA} for constant density. For closed-shell systems of constant density ($\rho_\alpha = \rho_\beta = \rho/2$), H^{OP} is given as [54]

$$H^{\mathrm{OP}}[\rho] = \frac{2.4103 q_{\alpha\beta}\rho^{1/3} + 0.5764}{6.2990 q_{\alpha\beta}^4\rho^{4/3} + 5.1053 q_{\alpha\beta}^3\rho + 0.79887 q_{\alpha\beta}^2\rho}. \tag{126}$$

By the quantum Monte Carlo method, the exact correlation energies were calculated for a spin-compensated uniform electron gas [95]. In agreement with the results, H^{OP} approaches zero as $O(\rho^{-1})$ would in the high-density limit and scales as $O(\rho^{-2/3})$ would in the low-density limit for a constant density.

(F) In a slowly varying limit ($x_\sigma \to 0$), T_σ is exactly expanded as [96]

$$\lim_{x_\sigma\to 0} T_\sigma = \frac{3}{5}(6\pi^2)^{2/3} + \frac{x_\sigma^2}{36} + O(x_\sigma^4). \tag{127}$$

Surprisingly, it is proved that K_σ^{P} can be expanded for this T_σ as

$$\lim_{x_\sigma\to 0} K_\sigma^{\mathrm{TFW}-\tau_\sigma} = 3\left(\frac{3}{4\pi}\right)^{1/3}\left(1 + \frac{5}{81(6\pi^2)^{2/3}}x_\sigma^2 + O(x_\sigma^4)\right), \tag{128}$$

which gives exactly twice the conventional exact gradient expansion coefficient, $5/162(6\pi^2)^{2/3}$ [97]. However, we suspect that the conventional coefficient is incorrectly halved because empirical observations [71] and conventional exchange functionals have given larger coefficients that are close to $5/81(6\pi^2)^{2/3} = 0.004063$, e.g. 0.004514 in B88 and 0.003612 in PBR. This remains to be proven. In any case, H^{OP} can be expanded for closed-shell systems in this limit as [98]

$$\lim_{x\to 0} H^{\mathrm{OP}}[\rho] = c_1[\rho] + c_2[\rho]x^2 + O(x^4), \tag{129}$$

where $c_p[\rho]$ ($p = 1, 2$) are functionals of only the electron density and $x = |\nabla\rho|/\rho^{4/3}$. Dimensional analysis [54] showed that both c_1 and c_2 of H^{OP} properly scale as $O(\rho^{-1})$ would in the high-density limit and as $O(\rho^{-2/3})$ would in the low-density limit.

(G) For density $\rho_q = q\rho_1$ of a q-electron system ($0 < q \leq 1$), T_σ scales as $O(\rho^{2/3})$ because of Eq. (102), where ρ_1 is the density for a one-electron system. Since K_σ^P scales as $O(\rho^{-2/3})$ for this T_σ, the Pfree exchange functional in Eq. (108) satisfies the necessary condition for being self-interaction free[99],

$$E_x[q\rho_1] = q^2 E_x[\rho_1]. \tag{130}$$

Table 11
Deviations of calculated Pfree exchange energies in hartree and calculated OP correlation energies in mhartree for the ground states of atoms. Mean Δ and MAE indicate mean deviation and mean absolute deviation respectively

	TFW	LLP	Thakker	TFλW	NLLP
Pfree exchange energies					
Mean Δ_{H-Ne}	0.109	0.056	0.099	0.038	0.006
Mean Δ_{Na-Ar}	0.211	0.262	0.280	0.005	−0.013
Total mean Δ	0.154	0.147	0.182	0.024	0.015
MAE_{H-Ne}	0.109	0.056	0.099	0.040	0.016
MAE_{H-Ne}	0.211	0.262	0.280	0.006	0.013
Total MAE	0.154	0.147	0.179	0.023	−0.002
OP correlation energies					
Mean Δ_{H-Ne}	−11.13	−3.74	−7.80	−8.54	−4.77
Mean Δ_{Na-Ar}	−7.81	−3.64	−6.78	−6.05	−3.95
Total mean Δ	−9.65	−3.69	−7.35	−7.43	−4.41
MAE_{H-Ne}	12.41	6.44	9.40	10.21	7.38
MAE_{H-Ne}	7.82	3.64	6.78	6.05	3.96
Total MAE	10.37	5.20	8.24	8.36	5.86

As far as we know, no other functional obeys this condition [100]. In addition, the OP correlation functional in Eq. (100) is definitely self-interaction free because it approaches zero as $O(\rho_\beta^{1/3})$ would for $\rho_\beta \to 0$.

(H) In a rapidly varying limit ($x_\sigma \to \infty$), T_σ increases as [96]

$$\lim_{x_\sigma \to \infty} T_\sigma = \frac{x_\sigma^2}{4}. \tag{131}$$

K_σ^{P} reduces asymptotically to zero for this T_σ as

$$\lim_{x_\sigma \to \infty} K_\sigma^{\mathrm{P}} = \frac{136}{5x_\sigma^2}, \tag{132}$$

and H^{OP} rapidly dilates as $O(x_\sigma^6)$. The Lieb–Oxford bound [100,101], $K_\sigma^{\mathrm{P}} < 4.231$, may be satisfied by a natural K_σ that obeys Eqs. (128) and (132). However, we indicated that K_σ must not approach zero for any x_σ [100] in order to obey the empirical rule that exchange energy is dominant in the exchange-correlation contribution for a rapidly varying density [72]. In the density tail ($R \to \infty$), the density changes rapidly, and, therefore, x_σ is large [96]. K_σ must satisfy the asymptotic relation for an exponentially decaying density in this region [102],

$$K_\sigma \to \frac{x_\sigma}{3\ln x_\sigma} (R \to \infty), \tag{133}$$

to reproduce the asymptotic behaviour of the exchange energy density, ϵ_x [102–106]:

$$\epsilon_x \to -\frac{1}{2R} (R \to \infty), \tag{134}$$

where ϵ_x is defined as $E_x \equiv \int \rho(\mathbf{R})\epsilon_x(\mathbf{R})\mathrm{d}^3\mathbf{R}$. The B88 exchange functional was developed to satisfy this asymptotic condition. In contrast with K_σ^{P} in Eq. (132), K_σ in Eq. (133) increases as $x_\sigma \to \infty$. What causes this discrepancy? We should notice that a functional in the form of Eq. (91) has been shown to disobey the asymptotic relation of the exchange potential [103],

$$v_x = \frac{\delta E_x}{\delta p} \to -\frac{1}{R} \quad (R \to \infty), \tag{135}$$

provided it obeys Eq. (134) [102]. Hence, we suspect that GGA-type exchange functionals do not inherently reproduce the nature of a rapidly varying density, including its long-range asymptotic behavior.

In conclusion, the fundamental conditions of kinetic, exchange, and correlation functionals are connected through T_σ, K_σ^{P}, and H^{OP} in Eqs. (109)–(111) with the exception of the rapidly-varying density limit (H). A study of the long-range exchange interaction might show the indicator how to satisfy condition (H), because the rapidly-varying limit is mostly dominated by this type of interaction. In any

Table 12
Deviations of calculated equilibrium geometries, atomization energies in kcal/mol, adiabatic electron affinities in eV, and ionization potentials in eV, for the G2-1 set of molecules by POP, BOP, and B3LYP functionals and the MP2 method. r_e is the atomic distance in Å and a is the bond angle in degree, respectively. All values were calculated with the 6-311++G(2p, 2d) basis set. MAE, mean Δ and max Δ indicate mean absolute deviation, mean deviation, and max deviation, respectively

	POP					BOP	B3LYP	MP2
	TFW	LLP	Thakker	TFλW	NLLP			
Equilibrium geometries								
MAE r_e	0.014	0.024	0.014	0.015	0.017	0.019	0.011	0.016
a	0.9	1.0	1.0	1.0	0.9	0.9	0.9	0.9
Max Δ r_e	0.152	0.098	0.065	0.129	0.074	0.072	0.078	0.101
a	5.1	5.3	5.9	4.9	4.6	4.7	6.4	5.1
Atomization energies								
MAE	22.6	4.1	9.5	18.3	7.7	3.1	3.0	10.5
Max Δ	55.0	15.7	22.2	45.9	19.6	12.3	20.2	29.5
Electron affinities								
MAE	0.21	0.18	0.12	0.22	0.11	0.12	0.11	0.26
Max Δ	0.52	0.29	0.24	0.55	0.47	0.36	0.55	0.74
Ionization potentials								
MAE	0.21	0.26	0.19	0.24	0.17	0.18	0.17	0.74
Max Δ	0.72	0.56	0.47	1.31	0.55	0.44	0.54	4.00

case, a general statement has not yet been given for the behavior of exchange functionals at this limit [96]. Hence, we can say that the remaining question is how to construct a kinetic energy functional that produces all these properties.

4.4. Calculations

4.4.1. Exchange and correlation energies of atoms

First, we calculated exchange and correlation energies of the ground states of 18 atoms, hydrogen through argon, using the Clementi HF Slater-type orbitals [106]. The 50-point Euler–Maclaurin quadrature [107,108] and the 194-point Lebedev quadrature [109,110] are used for radial and angle grids, respectively, in the numerical integrations. For the exact values, we used the numerical HF exchange energies [111] and the non-relativistic correlation energies of the exact great nuclear charge limits [112,113]. In the Pfree exchange energy calculations, we examined several types of conventional kinetic energy functionals, TFW, LLP, Thakker, TFλW, and NLLP, that are detailed in the Appendix. The Pfree exchange functional, Eq. (105), has a progressive part that can

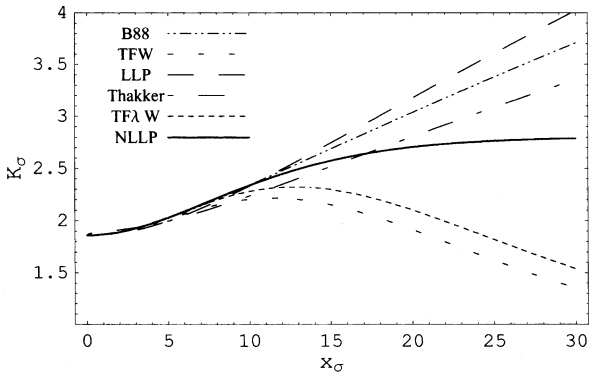

Fig. 10. The dependency of K_σ for a dimensionless parameter x_σ.

Table 13
Atomization energies of the dimers of the first-row transitions metals in eV. The relativistic correction and the zero-point vibration correction are incorporated. The underlined results correspond to those of the ground states of each dimer. Conventional high-level ab initio MO results are also given for comparison

Dimer	State	Dissociation limit	Exp.	BOP	B3LYP	B88	MP2	High-level ab initio MO
Sc_2	$^5\Sigma_u^-$	^2D–^4F	1.04 ± 0.22	1.92	1.36	1.35	2.00	0.59 (MRSDQCI)
Ti_2	$^3\Delta_g$	^5F–^5F	1.54 ± 0.19	2.79	1.77	0.43	unbound[a]	–
	$^7\Sigma_u^+$	^3F–^5F	–	2.03	0.55	1.43	no conv.[b]	0.94 (ACPF)
V_2	$^3\Sigma_g^-$	^6D–^6D	2.75	3.38	1.45	0.26	unbound[a]	–
Cr_2	$^1\Sigma_g^+$	^7S–^7S	1.53 ± 0.06	1.56	− 1.53	− 2.46	unbound[a]	1.58 (CASPT2)
Mn_2	$^1\Sigma_g^+$	^6S–^6S	0.3 ± 0.3	unbound[a]	unbound[a]	unbound[a]	unbound[a]	–
Fe_2	$^7\Delta_g$	^5F–^5F	1.15 ± 0.09	2.49	0.98	1.49	0.31	3.17 (FE-CI)
	$^7\Sigma_u^+$	^5F–^5F	–	no conv.[b]	1.38	no conv.[c]	1.09	–
Co_2	$^5\Delta_g$	^4F–^4F	–	2.45	0.42	1.30	1.23	–
	$^5\Sigma_g^+$	^4F–^4F	–	1.60	1.49	0.66	1.33	0.81 (SDCI)
Ni_2	$^3\Sigma_g^-$	^3D–^3D	2.04	2.67	1.48	1.86	− 2.28	1.78 (CASPT2)
	$^3\Sigma_g^+$	^3D–^3D	–	2.13	1.96	1.56	1.87	1.80 (CASPT2)
Cu_2	$^1\Sigma_g^+$	^2S–^2S	2.06 ± 0.03	2.16	2.03	1.61	1.99	1.97 (CASPT2)
Mean absolute Δ[c]			–	0.65	0.69	1.02	0.92	(0.947)
Max Δ[c]			–	1.34	− 3.06	− 3.99	− 2.75	(1.93)

[a] The ground states of these dimers are not bound for the method of calculation.
[b] We cannot get a convergent result for these states in the Kohn–Sham calculation.
[c] The deviations are taken for the ground states that are predicted for each method. The atomization energies of the unbound states are incorporated as zero.

be updated for kinetic energy density τ_σ. For the calculations of the OP correlation energies, we determined the parameter $q_{\alpha\beta}$ to reproduce the exact correlation energy of the Ar atom: 2.3897 for TFW, 2.3924 for LLP, 2.3895 for Thakker, 2.3665 for TFλW, and 2.3653 for NLLP.

Table 11 shows the deviations of calculated exchange energies for the ground state of the atoms [74]. The mean deviations show that the Pfree exchange energies are somewhat underestimated especially for the TFW, LLP, and Thakker functionals. The errors may be attributed to the omitted higher order terms, $(x_\sigma^2/\tau_\sigma)^n$ for $n \geq 2$ that may cause instability in practical evaluation. From the numerical point of view, we therefore have to develop an approach for evaluating the stable higher order values in order to connect conventional kinetic energy functionals with the Pfree exchange functional. The NLLP functional gives much more accurate exchange energies comparable to those of the B88 exchange functional [100]. On the other hand, the TFλW functional comparatively underestimates the Pfree energies, although it provides accurate energies within a margin of a few percent despite the parameter-free form. Since the shape of the TFλW and NLLP functionals are different especially for large x_σ, the underestimation may be due to the behavior of K_σ^P for large x_σ.

Table 11 also shows the deviations of calculated OP correlation energies [74]. We can see from the deviations that the LLP and NLLP functionals gave accurate OP correlation energies. Since these functionals give a sufficiently large K_σ^P for $5 < x_\sigma < 15$, T_σ in Eq. (109) for large x_σ ($x_\sigma > 5$) is essential to reproducing the well-balanced POP exchange-correlation energies of atoms, despite barely contributing to the kinetic energies themselves. In addition, these calculated OP correlation energies are much better than those of conventional other correlation functionals, e.g. LYP, PW91, PBE, and Filatov–Thiel (FT) correlation functionals [54]. The accurate energies mean that correlation contributions can be approximated by the interaction between two opposite-spin electrons that come close to each other.

4.4.2. Chemical properties of the G2 set

We applied the POP functional [74] to the calculations of equilibrium geometries, atomization energies,

Table 14
Atomization energies of the dimers of the second- and third-row transition metals in eV. The relativistic correction and the zero-point vibration correction are incorporated. The underlined results correspond to those of the ground states of each dimer

Molecule	State	Dissociation limit	Exp.	BOP	B3LYP	B88	MP2	High-level ab initio MO
Y_2	$^5\Sigma_u^-$	^2D–^4F	1.6	2.14	1.94	1.56	3.02	2.56 (full-CASSCF/SOC1)
Zr_2	$^3\Delta_g$	^5F–^5F	3.052 ± 0.001	3.68	3.24	1.06	6.19	–
	$^1\Sigma_g^+$	^5F–^5F	–	3.49	3.04	0.67	6.21	2.45 (MRSDCI)
	$^7\Sigma_g^+$	^3F–^5F	–	2.85	2.07	2.19	no conv.[a]	–
Nb_2	$^3\Sigma_g^-$	^6D–^6D	5.20	4.98	4.03	1.45	unbound[b]	2.24 (CASSCF)
	$^7\Delta_g$	^6D–^6D	–	2.61	1.94	0.37	4.49	–
Mo_2	$^1\Sigma_g^+$	^7S–^7S	4.74 ± 0.010	4.37	2.71	− 0.22	unbound[b]	–
Ru_2	$^7\Delta_u$	^5F–^5F	2.0 ± 0.2	3.25	2.20	1.91	5.04	2.0 (MRSDCI)
Rh_2	$^5\Delta_g$	^4F–^4F	2.4059 ± 0.005	3.00	1.76	1.79	unbound[b]	2.1 (CASSCF/MRCI/RCI)
	$^5\Sigma_g^+$	^4F–^4F	–	0.71	0.72	− 0.03	1.30	–
Pd_2	$^3\Sigma_u^+$	^1S–^3D	1.03 ± 0.16	1.96	1.70	1.56	1.83	1.86 (CASPT2)
	$^3\Sigma_g^-$	^3D–^3D	–	1.41	0.41	0.68	3.79	–
Ag_2	$^1\Sigma_g^+$	^2S–^2S	1.65 ± 0.03	1.53	1.52	1.04	2.05	1.96 (MRPT2)
The mean absolute deviation[c]			–	0.50	0.31	1.36	2.08	(0.82)
The max deviation[c]			–	1.05	− 1.76	− 4.69	− 4.47	(−2.96)
Pt_2	$^3\Sigma_g^-(\pi\pi)$	^3D–^3D	3.71 ± 0.16	3.80	3.24	2.96	4.34	3.82 (AIMP CASPT2)
	$^3\Sigma_g^-(\delta\delta)$	^3D–^3D	–	2.95	2.05	2.19	4.68	2.62 (PP CASPT2)
Au_2	$^1\Sigma_g^+$	^2S–^2S	2.29	2.61	2.57	2.11	3.17	2.19 (CCSD(T))
The mean absolute deviation[b]			–	0.79	0.72	1.03	1.04	0.31
The max deviation[b]			–	1.49	− 3.06	− 3.99	1.80	0.96

[a] We cannot get a convergent result for these states in the Kohn–Sham calculation.
[b] The ground states of these dimers are not bound for the method of calculation.
[c] The deviations are taken for the ground states that are predicted for each method.

electron affinities and ionization potentials of the G2-1 set of molecules [114] by the Kohn–Sham method using 6-311++G(2p, 2d) basis functions [115–117]. Zero-point vibrational frequencies were taken into account in the calculated energies. Table 12 shows the deviations of the calculated POP results for the TFW, LLP, Thakker, TFλW, and NLLP kinetic energy functionals. For comparison, we also present the calculated results of the B88 exchange + OP correlation (BOP) functional, the hybrid B3LYP functional, and the ab initio second-order Moller–Plesset perturbation method [54]. In Fig. 10, the x_σ-dependencies of K_σ^{P} in Eq. (110) are shown for these kinetic energy functionals.

For equilibrium geometries, almost equivalent results were obtained for all kinetic energy functionals in the POP functional. Even the TFW kinetic energy functional gives accurate POP results comparable to the B3LYP functional, despite the POP functional has only one parameter for this functional. It was, therefore, presumed that the accuracy of the calculated equilibrium geometries is determined by K_σ for the relatively small x_σ, similar to that of the exchange energies.

On the contrary, atomization energies were highly affected by the functional used [100]. In the POP functionals, the LLP functional provides the most accurate atomization energies followed by NLLP and Thakker. From Fig. 10, it was revealed that calculated atomization energies may have been influenced especially affected by K_σ in the region $12 < x_\sigma < 20$.

The calculated adiabatic electron affinities and ionization potentials were also highly affected by the shape of the functional used. In both calculations, NLLP and Thakker give accurate energies, while TFW, LLP, and TFλW estimate worse energies. We can see from Fig. 10 that the K_σs for a large x_σ affected on the affinities and the ionization potentials, because the major difference between the former and the latter seem to be in this region of x_σ. Hence, it was shown that K_σ for large x_σ is important for reproducing these properties.

4.4.3. Transition metal dimers

In order to explore the applicabilities of various kinds of density functionals, we calculated the atomization energies for the first- to third-row transition metal dimers [75,76]. Despite the very simple structures of dimers, it is difficult to reproduce these values, because the dimers have a different characteristic electron configuration for each ground state.

The calculation reported here were carried out by the unrestricted Kohn–Sham method [70]. The Wachters [118,119] +f [120] [14s11p6d3f]/(8s6p4d1f) Gaussian basis functions were employed for the first-row transition metals. For the second- and third-row metals, we used the generally-contracted well-tempered (23s18p15d4f/9s5p6d2f) basis set [121] [(23s16-13d4f/9s6p5d2f) only for Zr atom], and the non-relativistically optimized Gropen (19s16p11d7f/9s6p6d3f) basis set [122], respectively. In Tables 13 and 14, we present the calculated results of the BOP, B3LYP, and B88 functionals, and the MP2 method for comparison. The 94-point Euler–Maclaurin quadrature [118,119] and the 16×32-point Gauss–Legendre quadrature were used in the numerical integrations for radial and angular grids, respectively. Relativistic corrections (RC) were included by 'a relativistic scheme by eliminating small components (RESC) [43]. Calculated atomization energies were also corrected for zero-point vibrational frequencies.

The following features were evident from the calculated results for the dimers;

1. The BOP functional overestimates the atomization energies, and the errors tend to decrease as the number of outermost d electrons increases (from Sc_2 to Cr_2, from Fe_2 to Cu_2, from Y_2 to Mo_2, and from Ru_2 to Ag_2). This overestimation is related to the problem that density functionals tend to overstabilize the electron configurations that contain high-angular-momentum open-shell orbitals. However, the errors clearly decrease until they are less than those of high-level ab initio molecular orbital calculations.
2. The hybrid B3LYP functional considerably underestimates the atomization energy of V_2, Cr_2, Nb_2, and Mo_2, because it gives an erroneous energy gap between the configurations of fairly different spin multiplicity.
3. Dynamical electron correlations from the OP functional similarly shorten the bond lengths and raise the atomization energies for all dimers.

After all, we found that the lack of the long-range

exchange interaction between the outermost s and d orbitals may be responsible for the overstabilization problem of density functionals for electron configurations containing high-angular-momentum open-shell orbitals in transition metals. This problem seems to be partly corrected by combining the Hartree–Fock exchange integral with the exchange functional, just like in the hybrid B3LYP functional. However, this combination was found to cause a new problem that the hybrid functional provides poor energy gaps between states whose spin multiplicities are quite different. The question to consider now is how to incorporate the long-range exchange interaction into exchange functionals while maintaining a balance between exchange and correlation contributions.

Appendix A. Kinetic energy functionals

Conventional kinetic energy functionals are mostly described in a GGA form [123,124]

$$T_s = \frac{1}{2}\sum_\sigma \int \tau_\sigma \mathrm{d}^3\mathbf{R} = \frac{1}{2}\sum_\sigma \int \rho_\sigma^{5/3} T_\sigma \mathrm{d}^3\mathbf{R}, \qquad \text{(A1)}$$

where T_σ is usually a dimensionless functional of x_σ. The local spin density approximations (LSDA) of T_σ is that of the Thomas–Fermi kinetic energy functional,

$$T_\sigma^{LSDA} = \frac{3}{5}(6\pi^2)^{2/3}. \qquad \text{(A2)}$$

The Thomas–Fermi–Weizsäcker second-order gradient correction (TFW) is given as [71]

$$T_\sigma^{TFW} = T_\sigma^{LSDA} + \frac{x_\sigma^2}{36}. \qquad \text{(A3)}$$

A kinetic energy functional was suggested by Lee, Lee and Parr [125] (LLP) from an analogy to the Becke exchange functional [53] (B88):

$$T_\sigma^{LLP} = T_\sigma^{\mathrm{LSDA}}\left(1 + \frac{0.0044188 x_\sigma^2}{1 + 0.0253 x_\sigma \sinh^{-1} x_\sigma}\right). \qquad \text{(A4)}$$

Thakker [123] added the Ou–Yang–Levy term [126] to the LLP functional with an empirical fit:

$$T_\sigma^{\mathrm{Thakker}} = T_\sigma^{\mathrm{LSDA}} \times\left(1 + \frac{0.0055 x_\sigma^2}{1 + 0.0253 x_\sigma \sinh^{-1} x_\sigma} - \frac{0.072 x_\sigma}{1 + 2^{5/3} x_\sigma}\right). \qquad \text{(A5)}$$

We suggested two types of kinetic energy functionals as techniques for recovering the numerical accuracy of the Pfree exchange functional. One is the Thomas–Fermi-λ Weizsäcker (TFλW) functional [71],

$$T_\sigma^{\mathrm{TF\lambda W}} = T_\sigma^{\mathrm{LSDA}} + \frac{\lambda x_\sigma^2}{36}, \qquad \text{(A6)}$$

where parameter λ is set to 0.8945, and the other is the LLP-type (NLLP) functional, which meets the fundamental conditions of the exact kinetic energy functional except for rapidly-varying density and self-interaction-free ones,

$$T_\sigma^{\mathrm{NLLP}} = T_\sigma^{\mathrm{LSDA}} + \frac{x_\sigma^2}{36(1 + c_{\mathrm{NLLP}} x_\sigma \sinh^{-1} x_\sigma)}, \qquad \text{(A7)}$$

where parameter c_{NLLP} is set to 0.0075, so as to reproduce the exact exchange energy of the Ar atom by the Pfree functional.

References

[1] K. Hirao, Chem. Phys. Lett. 190 (1992) 374.
[2] K. Hirao, Chem. Phys. Lett. 196 (1992) 397.
[3] K. Hirao, Chem. Phys. Lett. 201 (1993) 59.
[4] K. Hirao, Intern. J. Quantum Chem. S 26 (1992) 517.
[5] H. Nakano, J. Chem. Phys. 99 (1993) 9873.
[6] H. Nakano, Chem. Phys. Lett. 207 (1993) 372.
[7] H. Nakano, K. Nakayama, K. Hirao, M. Dupuis, J. Chem. Phys. 106 (1997) 4912.
[8] W.F. Polik, D.R. Guyer, C.B. Moore, J. Chem. Phys. 92 (1990) 3453.
[9] G.E. Scuseria, H.F. Schaefer III, J. Chem. Phys. 90 (1989) 3629.
[10] T.H. Dunning Jr., J. Chem. Phys. 90 (1989) 1007.
[11] H. Nakano, T. Tsuneda, T. Hashimoto, K. Hirao, J. Chem. Phys. 104 (1996) 2312.
[12] T.H. Dunning Jr, P.J. Hay, in: H.F. Schaefer (Ed.), Methods of Electronic Structure Theory, vol. 3, Plenum Press, New York, 1977, p. 1.
[13] L. Serrano-Andres, M. Merchan, I. Nebot-Gil, B.O. Roos, M. Fulscher, J. Am. Chem. Soc. 115 (1993) 6184.
[14] O. Christiansen, P. Jørgensen, J. Am. Chem. Soc. 120 (1998) 3423.

[15] J. Wan, J. Meller, M. Hada, M. Ehara, H. Nakatsuji, J. Chem. Phys. 113 (2000) 7853.
[16] L.W. Pickett, J. Chem. Phys. 8 (1940) 293.
[17] L.W. Pickett, N.J. Hoeflich, T.C. Liu, J. Am. Chem. Soc. 73 (1951) 4865.
[18] W.M. Flicker, O.A. Mosher, A. Kuppermann, Chem. Phys. Lett. 38 (1976) 489.
[19] W.M. Flicker, O.A. Mosher, A. Kuppermann, J. Chem. Phys. 64 (1976) 1315.
[20] M.B. Robin, Higher Excited States of Polyatomic Molecules, Academic Press, London, vol. 2 1975.
[21] C.D. Cooper, A.D. Williamson, J.C. Miller,, N. Compton, J. Chem. Phys. 73 (1980) 1527.
[22] P.J. Derrick, L. Asbrink, O. Edqvist, B.O. Jonsson, E. Lindholm, Int. J. Mass Spectrom. Ion Phys. 6 (1971) 161.
[23] J.L. Roebber, D.P. Gerrity, R. Hemley, V. Vaida, Chem. Phys. Lett. 75 (1980) 104.
[24] H. Nakano, K. Hirao, Chem. Phys. Lett. 317 (2000) 90.
[25] K.P. Huber, G. Herzberg, Molecular Spectra Structure: Constants of Diatomic Molecules, Van Nostrand Reinhold, New York, 1979.
[26] H. Nakano, J. Nakatani, K. Hirao, J. Chem. Phys. 114 (2001) 1133.
[27] H. Nakano, K. Hirao, M.S. Gordon, J. Chem. Phys. 108 (1998) 5660.
[28] H. Nakano, N. Otsuka, K. Hirao, in: K. Hirao (Ed.), Recent Advances in Computational Chemistry, vol. 4, Recent Advances in Multireference Methods, World Scientific, Singapore, 1999, p. 131.
[29] T.U. Helgaker, P. Jørgensen, Adv. Quantum Chem. 19 (1988) 183.
[30] P. Jørgensen, T.U. Helgaker, J. Chem. Phys. 89 (1988) 1560.
[31] K. Hirao, H. Nakano, K. Nakayama, M. Dupuis, J. Chem. Phys. 105 (1996) 9227.
[32] K. Hirao, H. Nakano, K. Nakayama, J. Chem. Phys. 107 (1997) 9966.
[33] J.M. Foster, S.F. Boys, Rev. Mod. Phys. 32 (1960) 300.
[34] K. Ruedenberg, M.W. Schmidt, M.M. Gilbert, S.T. Elbert, Chem. Phys. 71 (1982) 41.
[35] K. Ruedenberg, M.W. Schmidt, M.M. Gilbert, Chem. Phys. 71 (1982) 51.
[36] K. Ruedenberg, M.W. Schmidt, M.M. Gilbert, S.T. Elbert, Chem. Phys. 71 (1982) 65.
[37] H. Nakano, K. Nakayama, K. Hirao, J. Mol. Struct. (Theochem) 461–462 (1999) 55.
[38] P. Pyykkö, Chem. Rev. 88 (1988) 563.
[39] H.A. Bethe, E.E. Salpeter, Quantum Mechanics of One- and Two-electron Atoms, Springer, Berlin, Heidelberg, New York, 1957.
[40] L.L. Foldy, S.A. Wouthuysen, Phys. Rev. 78 (1950) 9.
[41] E. van Lenthe, E.J. Baerends, J.G. Snijders, J. Chem. Phys. 99 (1993) 4597.
[42] Ch. Chang, M. Pelissier, Ph. Durand, Phys. Scr. 34 (1986) 394.
[43] T. Nakajima, K. Hirao, Chem. Phys. Lett. 302 (1999) 383.
[44] T. Nakajima, T. Suzumura, K. Hirao, Chem. Phys. Lett. 304 (1999) 271.
[45] T. Nakajima, K. Hirao, J. Chem. Phys. 113 (2000) 7786.
[46] T. Nakajima, K. Hirao, Chem. Phys. Lett. 329 (2000) 511.
[47] R.J. Buenker, P. Chandra, B.A. Hess, Chem. Phys. 84 (1984) 1.
[48] B.A. Hess, Phys. Rev. A 33 (1986) 3742.
[49] M. Douglas, N.M. Kroll, Ann. Phys. (N.Y.) 82 (1974) 89.
[50] G. Jansen, B.A. Hess, Phys. Rev. A 39 (1989) 6016.
[51] T. Suzumura, T. Nakajima, K. Hirao, Intern. J. Quantum Chem. 75 (1999) 757.
[52] K. Hirao, K. Nakayama, T. Nakajima, H. Nakano, Computational Chemistry, in: J. Lesczynski (Ed.), World Scientific, Singapore, 1999, p. 227.
[53] A.S. Becke, Phys. Rev. A 38 (1988) 3098.
[54] T. Tsuneda, T. Suzumura, K. Hirao, J. Chem. Phys. 110 (1999) 10664.
[55] C. Lee, W. Yang, R.G. Parr, Phys. Rev. B 37 (1988) 785.
[56] A.D. Becke, J. Chem. Phys. 98 (1993) 5684.
[57] T. Nakajima, K. Koga, K. Hirao, J. Chem. Phys. 112 (2000) 10142.
[58] P. Burroughs, S. Evans, A. Hammett, A.F. Orchard, N.V. Richardson, J. Chem. Soc. Faraday Trans. 270 (1974) 1895.
[59] Y.-K. Choe, T. Nakajima, K. Hirao, R. Lindh, J. Chem. Phys. 111 (1999) 3837.
[60] H. Witek, T. Nakajima, K. Hirao, J. Chem. Phys. 113 (2000) 8015.
[61] Y. Kayaki, H. Tsukamoto, M. Kaneko, I. Shimizu, A. Yamamoto, M. Tachikawa, T. Nakajima, J. Organometal. Chem. 622 (2001) 199.
[62] S. Yanagisawa, T. Nakajima, T. Tsuneda, K. Hirao, Mol. Struct. (Theochem) 537 (2001) 63.
[63] K. Motegi, T. Nakajima, K. Hirao, L. Seijo, J. Chem. Phys. 114 (2001) 6000.
[64] D. Fedorov, T. Nakajima, K. Hirao, Chem. Phys. Lett. 335 (2001) 183.
[65] K. Molzberger, W.H.E. Schwarz, Theor. Chim. Acta 94 (1996) 213.
[66] J. Sucher, Phys. Rev. A 22 (1980) 348.
[67] R. Samzow, B.A. Hess, G. Jansen, J. Chem. Phys. 96 (1992) 1227.
[68] M. Seth, P. Schwerdtfeger, M. Dolg, J. Chem. Phys. 106 (1997) 3623.
[69] M. Seth, P. Schwerdtfeger, K. Faegri, J. Chem. Phys. 111 (1999) 6422.
[70] W. Kohn, L.J. Sham, Phys. Rev. A 140 (1965) 1133.
[71] R.G. Parr, W. Yang, Density-Functional Theory of Atoms and Molecules, Oxford University Press, New York, 1989.
[72] J.P. Perdew, K. Burke, M. Ernzerhof, Phys. Rev. Lett. 77 (1996) 3865.
[73] T. Tsuneda, K. Hirao, Phys. Rev. B 62 (2000) 15527.
[74] T. Tsuneda, M. Kamiya, N. Morinaga, K. Hirao, J. Chem. Phys. 114 (2001) 6505.
[75] S. Yanagisawa, T. Tsuneda, K. Hirao, J. Chem. Phys. 112 (2000) 545.
[76] S. Yanagisawa, T. Tsuneda, K. Hirao, submitted.
[77] T. Tsuneda, K. Hirao, Chem. Phys. Lett. 268 (1997) 510.
[78] R. Colle, O. Salvetti, Theoret. Chim. Acta 37 (1975) 329.
[79] A.K. Rajagopal, J.C. Kimball, M. Banerjee, Phys. Rev. B 18 (1978) 2339.

[80] A.K. Rajagopal, Adv. Chem. Phys. 41 (1980) 59.
[81] A.D. Becke, J. Chem. Phys. 88 (1988) 1053.
[82] J.W. Negele, D. Vautherin, Phys. Rev. C 5 (1972) 1472.
[83] R.M. Koehl, G.K. Odom, G.E. Scuseria, Mol. Phys. 87 (1996) 835.
[84] T.V. Voorhis, G.E. Scuseria, Mol. Phys. 92 (1997) 601.
[85] T.V. Voorhis, G.E. Scuseria, J. Chem. Phys. 109 (1998) 400.
[86] J.C. Slater, Phys. Rev. 81 (1951) 385.
[87] S.H. Vosko, L. Wilk, M. Nusair, Can. J. Phys. 58 (1980) 1200.
[88] J.P. Perdew, Y. Wang, Electronic Structure of Solids '91, in: P. Ziesche, H. Eschrig (Eds.), Akademie Verlag, Berlin, 1991.
[89] M. Levy, J.P. Perdew, Phys. Rev. A 32 (1985) 2010.
[90] H. Ou-Yang, M. Levy, Phys. Rev. A 42 (1990) 155.
[91] M. Levy, Phys. Rev. A 43 (1991) 4637.
[92] M. Levy, J.P. Perdew, Int. J. Quantum Chem. 49 (1994) 539.
[93] M. Levy, J.P. Perdew, Phys. Rev. B 48 (1993) 11638.
[94] A. Gorling, M. Levy, Phys. Rev. A 45 (1992) 1509.
[95] D.M. Ceperley, B.J. Alder, Phys. Rev. Lett. 45 (1980) 566.
[96] R.M. Dreizler, E.K.U. Gross, Density-functional Theory: an Approach to the Quantum Many-Body Problem, Springer-Verlag, Berlin, Heidelberg, 1990.
[97] L. Kleinman, S. Lee, Phys. Rev. B 37 (1988) 4634.
[98] S.-K. Ma, K.A. Brueckner, Phys. Rev. 165 (1968) 18.
[99] Y. Zhang, W. Yang, J. Chem. Phys. 109 (1998) 2604.
[100] T. Tsuneda, T. Suzumura, K. Hirao, J. Chem. Phys. 111 (1999) 5656.
[101] E.H. Lieb, S. Oxford, Int. J. Quantum Chem. 19 (1981) 427.
[102] R. van Leeuwen, E.J. Baerends, Phys. Rev. A 49 (1994) 2421.
[103] M. Levy, J.P. Perdew, V. Sahni, Phys. Rev. A 30 (1984) 2745.
[104] H. Chermette, A. Lembarki, H. Razafinjanahary, F. Rogemond, Advances in Quantum Chemistry, 33, Academic Press, San Diego, 1998.
[105] N.H. March, Phys. Rev. A 36 (1987) 5077.
[106] E. Clementi, Tables of Atomic Functions, supplement to E. Clementi, IBM J. Res. Develop. 9 (1965) 2.
[107] C.W. Murray, N.C. Handy, G.J. Laming, Mol. Phys. 78 (1993) 997.
[108] M.W. Gill, B.G. Johnson, J.A. Pople, M.J. Frisch, Chem. Phys. Lett. 197 (1992) 499.
[109] V.I. Lebedev, Zh. Vychisl. Mat. Fiz. 15 (1975) 48 (English translation in U.S.S.R. Comput. Math. and Math. Phys.).
[110] V.I. Lebedev, Zh. Vychisl. Mat. Fiz. 16 (1976) 293 (English translation in U.S.S.R. Comput. Math. and Math. Phys.).
[111] J.P. Perdew, J.A. Chevary, S.H. Vosko, K.A. Jackson, M.R. Pederson, D.J. Singh, C. Fiolais, Phys. Rev. B 46 (1992) 6671.
[112] S.J. Chakravorty, S.R. Gwaltney, E.R. Davidson, F.A. Parpia, C.F. Fischer, Phys. Rev. A 47 (1993) 3649.
[113] S.J. Chakravorty, E.R. Davidson, J. Phys. Chem. 100 (1996) 6167.
[114] L.A. Curtiss, K. Raghavachari, G.W. Trucks, J.A. Pople, J. Chem. Phys. 94 (7221) 1991 and references therein.
[115] R. Krishnan, J.S. Binkley, R. Seeger, J.A. Pople, J. Chem. Phys. 72 (1980) 650.
[116] A.D. McLean, G.S. Chandler, J. Chem. Phys. 72 (1980) 5639.
[117] M.J. Frisch, J.A. Pople, J.S. Binkley, J. Chem. Phys. 80 (1984) 3265.
[118] A.J.H. Wachters, J. Chem. Phys. 52 (1970) 1033.
[119] A.J.H. Wachters, IBM Tech. Report RJ584, 1969.
[120] C.W. Bauschlicher Jr. S. R, L. anghoff, L.A. Barnes, J. Chem. Phys. 91 (1989) 2399.
[121] S. Huzinaga, M. Klobukowski, J. Mol. Struct. (Theochem) 167 (1988) 1.
[122] O. Gropen, J. Comp. Chem. 8 (1987) 982.
[123] A.J. Thakker, Phys. Rev. A 46 (1992) 6920.
[124] D.J. Lacks, R.G. Gordon, J. Chem. Phys. 100 (1994) 4446.
[125] H. Lee, C. Lee, R.G. Parr, Phys. Rev. A 44 (1991) 768.
[126] H. Ou-Yang, M. Levy, Int. J. Quantum Chem. 40 (1991) 379.